Manufacturing Techniques Using Femtosecond Lasers in Transparent Materials

by

Yonghyun Cho
Bachelor of Engineering, Halla University, 2008

A Thesis Submitted in Partial Fulfillment
of the Requirements for the Degree of

MASTER OF APPLIED SCIENCE

in the Department of Mechanical Engineering

Supervisory Committee

Manufacturing Techniques Using Femtosecond Lasers in Transparent Materials

by

Yonghyun Cho
BEng, Halla University, 2008

Supervisory Committee

Dr. Colin Bradley, Department of Mechanical Engineering
Co-Supervisor

Dr. Ben Nadler, Department of Mechanical Engineering
Co-Supervisor

Abstract

Supervisory Committee

Dr. Colin Bradley, Department of Mechanical Engineering
Co-**Supervisor**

Dr. Ben Nadler, Department of Mechanical Engineering
Co-Supervisor

Femtosecond laser direct writing in transparent materials such as glass and optical fibers has been used as a versatile tool in order to fabricate various 3-D photonic structures such as active and passive waveguides, couplers, gratings and diffractive optical elements (DOEs). This capability of patterning and refractive index modification in the bulk of transparent materials depends on the nonlinear absorption phenomenon. This practical technique has the potential to be used for cost effective and simplified manufacturing in various applications. This thesis examines three advanced manufacturing techniques that use ultrashort pulse filamentary propagation induced by nonlinear absorption in the transparent materials. First, a new gradient index lens fabrication method using femtosecond laser direct writing is introduced. Light that passes through the lens with refractive index change resulting from localized energy deposition is focused using a beam profiler. Second, wide welding area of glass samples are used to fabricate microfluidic devices with long channels by adopting customized fixture. The fixture making artificial pressure helps the two glass samples have wide optical contact area and the highly intensive pulse filamentation strongly joins glass slides. As an example of a more specific application, microfluidic samples with long grooves sealed by femtosecond laser welding were successfully fabricated as part of this project. Finally, a screw-shaped, long-period grating sensor was fabricated by rotating the optical fiber. This technique enables the

fiber core to have asymmetric refractive index change, resulting in higher sensitivity compared to conventional long period grating sensors. Also, a new long-period grating sensor with reverse bending effect has been demonstrated by producing complex pitches of refractive index change.

Table of Contents

List of Figures

Acknowledgments

I gratefully acknowledge the motivation, support, and assistance I received from Dr. Colin Bradley and Dr. Ben Nadler as an MASc student at the University of Victoria. They really care of me whenever I was in trouble so I was able to achieve academic results. Also, Dr. Jun was a great academic supervisor giving me many academic ideas. By pursuing Dr. Jun's advice, both intellectual and personal in nature, I was able to settle down in Canada.

I thank everyone who pursued studies with me in the laboratory of advanced multi-scale manufacturing (LAMM). I thank Jung-Hyuk Ko and Farid Ahmed for giving me advice throughout my MASc study. Moreover, I appreciate all the technical help from, Vahid Ahsani, Kaveh Nazeri, Salah Elfurjani, Young-Keun Hong,and Max Rukosuyev. I thank Ahmad Esmaelirad and Syed Ali Baqar for all their encouragement.

I would also like to thank my parents and sister for the support they provided me through my entire life. In particular, I was lucky to have constant love and support from my parents no matter the situation. I must acknowledge, finally, the many faculty members who have cooperated with me on many projects.

Chapter 1: Introduction

A variety of research projects have investigated material processing, biomedical devices, sensing systems, chemical analysis and a wide-range of scientific applications since the invention of lasers in 1960 [1]. Since that time, ultrashort pulsed laser systems have been developed not only to generate high peak power but also to minimize damage and heat affected zones for improved performance [2, 3]. In the long-pulse method, machining is carried out through the evaporation of material in the work surface. The pulse duration of long-pulse lasers is longer than the heat diffusion time [4]. Therefore, it is hard to accumulate threshold heat that would result in material damage. The energy delivered by a laser pulse easily diffuses before the next pulse strikes the machining spot. Instead of plasma, material in the work surface is driven into its molten phase. Consequently, diffused heat influences the morphology of machining and is one of the key parameters for the quality of micromachining [5, 6]. The efficiency of the machining process by long-pulse lasers is accordingly reduced due to the escape of energy from the work surface. For this reason, it is hard to precisely micro-machine materials which are good conductors of heat. Moreover, heat diffusion does not allow the working temperature to raise much beyond the melting point of the sample material. Therefore, a molten zone is reached in the work surface instead of producing a plasma state. Molten material in the work surface keeps boiling due to the nonstop striking of laser pulses. Ejected drops of the molten material contaminate the sample [7] .

Elimination of such contaminants is usually very difficult without damaging the sample. As well as the efficiency reduction and sample contamination, heat diffusion leads to several unintended phenomena such as surface ripple and reduced machining accuracy. Diffused heat expands the molten zone so it is much larger than the beam spot. Consequently, it is not possible to machine micron features with long-pulse lasers. Heat diffusion results in numerous undesirable side effects, such as heat affected zone, shock wave, and micro-cracks that reduce the quality of machining [8]. For instance, the cracks introduced sometimes travel beyond the machining zone and destroy adjacent structures (typically 10μm – 1mm) [9]. Ultrashort pulse lasers, however, can successfully overcome the drawbacks of long-pulse lasers. Their ablation process reduces the unexpected phenomena that take place in the case of long-pulse laser machining. The short pulse duration of femtosecond lasers inhibits heat diffusion from the work spot of the sample material. As a result, pulse energy accumulates and immediately raises the working temperature beyond the evaporation point of the material [10]. In fact, temperatures continue increasing until the material enters the plasma state. Plasma state has very high power density that few metals can withstand. Therefore, it is possible to machine any material easily with high-precision using femtosecond lasers. Thus, the ultrashort-pulse lasers open new research areas in ultrafast optics, encouraging research groups all over the world. Ultrashort-pulse lasers have an advantage compared to conventional lasers. Extremely high intensity can be produced by the focused ultrashort laser pulses. As a result, technologies of light-matter interactions such as table-top ultrafast generation, filament propagation in air and ultrafast laser material processing can be achieved [11-13].

This thesis focuses on advanced manufacturing techniques using ultrashort laser pulse interaction with transparent materials. Hirao fabricated optical waveguides inside glass materials using femtosecond laser pulses in 1996 [13]. Sub-micrometer sized refractive index inside transparent materials was modified storing three-dimensional data for engraving very fine-scale patterns inside transparent materials such as fused silica, fused quartz, sapphire and BK7 optical glass [14]. Since this original study of refractive index modification inside transparent materials, various applications have been investigated by researchers: such as laser surgery [15], integrated optics [16], three dimensional micro-structuring [17], and optical data storage using ultrashort- pulse laser [18]. Moreover, the first demonstration of long-period fiber Bragg gratings has attracted significant attention in the field of fiber optic sensors [19]. Also, nonlinear absorption phenomenon has been shown to enable the joining of transparent materials without any intermediate material [20]. Despite these advantages of ultrashort pulse induced modification in transparent materials, it is still challenging to apply this mechanism in practice due to the complex fabrication methods, which require very sensitive work on the laser parameters such as power, irradiation time and sample preparation of various transparent materials.

The main objective of this thesis is to introduce advanced fabrication techniques using femtosecond laser pulse induced machining in transparent materials for optical devices.

1.1 Femtosecond laser direct writing technique

Due to its straightforward fabrication method and flexibility, femtosecond laser direct writing (FLDW) has been employed in various applications requiring material processing in transparent materials. Figure 1.1 shows the femtosecond laser direct writing process that creates 3-D structures.

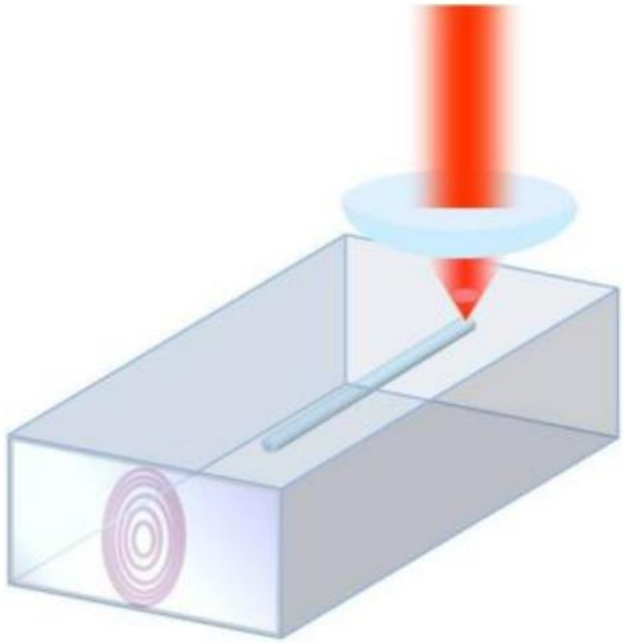

Figure 1.1 Schematic of femtosecond laser pulse induced material modification in a transparent material [21].

The unique and distinct feature of 3-D material modification using femtosecond laser direct writing is achieved by nonlinear absorption processes under ultrahigh intensity. This localized high intensity of laser pulses produces 3-D volumetric structural changes in transparent materials. Moreover, the tightly focused beam produces controlled patterns

without additional process and expensive consumable parts such as post-heat treatment and photo masks. This enables manufacturers to fabricate customized devices and prototypes by simply creating the desired computerized scanning path and optical configuration. Femtosecond laser direct writing has been used as a versatile tool in the fabrication of various 3-D photonic structures such as active and passive waveguides [13], couplers [22], gratings [23], and diffractive optical elements (DOEs) [24]. This capability of patterning and refractive index modification in the bulk of transparent materials depends on the nonlinear absorption phenomenon discussed in Chapter 2. Figure 1.2 compares the nonlinear and linear absorption by embedded 3-D controlled patterning. An absorption band at the incident wavelength is shown in the material (a) while the nonlinear absorption localized within a focal volume occurs in the material (b). This confined nonlinear absorption occurs when the laser intensity exceeds the threshold of structural modification.

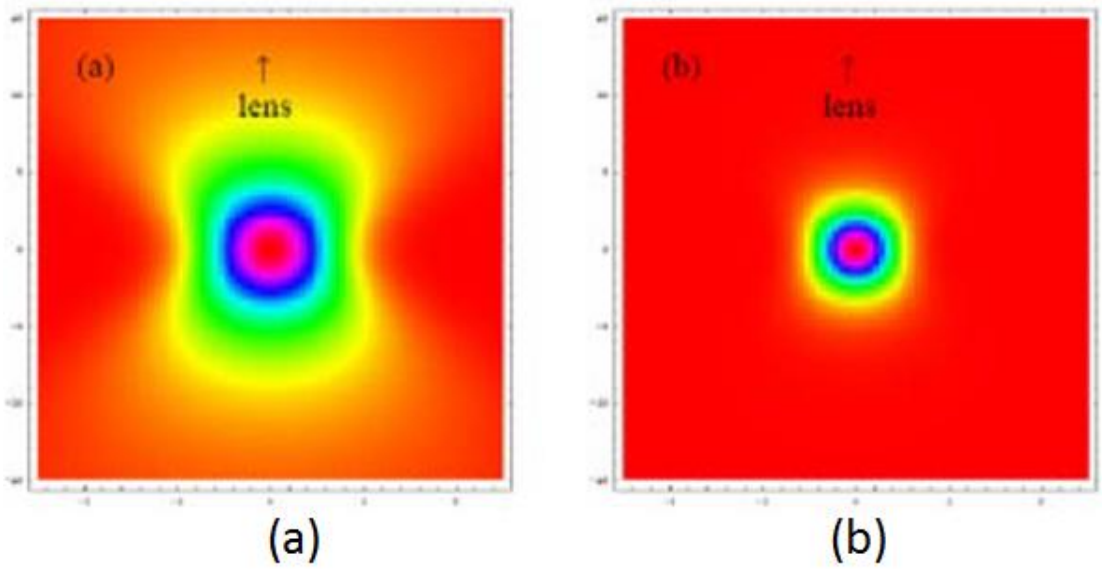

Figure 1.2: Schematic diagram of linear (a) and nonlinear absorption (b) in a transparent material [21].

High transparency materials and high intensity of the laser pulse are the requirements for nonlinear absorption to occur in glass materials. Under these circumstances, nonlinear absorption is confined when the laser beam is tightly focused in the transparent material, which is called filament. Filament can be used as an optical pen to modify the refractive index or to write new structures into transparent materials. Also, the tightly focused femtosecond laser beam can be controlled by external parameters such as laser power and numerical aperture of objective lens. In other words, the process of modifying structures in the transparent materials is highly dependent on optical components and irradiation schemes. Generally, the dimensions of gratings inside transparent materials and the laser induced refractive index changes are controlled by

laser parameters (wavelength, pulse width, power and repetition rate), mechanical parameters (scanning speed, precision of stage) and optical parameters (numerical aperture, beam reflection mirrors). With these controlled laser and optical parameter, pulse filamentation is achieved in glass materials and an important tool for the fabrications of various optical devices in this thesis.

1.2 Contribution

Three manufacturing techniques using transparent materials, such as glass and optical fibers, are introduced in this thesis. Each uses ultrashort pulse filamentation. Pulse filaments provide controlled pulse energy, enabling the fabrication of various optical devices such as microfluidic device and optical fiber sensors. Although there are plenty of methods to manufacture optical devices, they are either expensive or rely on complex processes. I propose a new concept of gradient index (GRIN) lens fabrication using thin glass plates and pulse filamentation. This method using femtosecond lasers has not yet been reported by other researchers, so only the concept viability and potential to improve manufacturing are demonstrated in this thesis. In addition, my experiments resulted in a wide welding area of glass samples when compared to other studies (maximum 1 x 1 cm). This was achieved by using customized fixtures and intense pulse filaments. Finally, highly sensitive long-period fiber grating sensors with symmetric refractive index change was fabricated by rotating the fiber and a new long period grating with complex helical

shape of refractive index change in the fiber was produced, which suggests possibilities for future applications.

1.3 Content summary

Chapter two presents the basic principles of nonlinear absorption and ionization that occur as a result of the interaction of ultrashort laser pulses with transparent materials.

Chapter three explains the refractive index change in glass materials using pulse filaments and is characterized according to pulse energy. The chapter also explains the new concept of gradient index lens fabrication method, which has been developed using controlled 3-D structuring of pulse filaments.

Chapter four demonstrates the joining of two glass slides with wide welding area, as demonstrated via a customized fixture. Experiments in this thesis achieved a relatively wide sealing area (418 mm^2) compared to previous work (1 cm^2) [25] .

Chapter five, I discuss how highly sensitive long period grating optical sensors were fabricated via screw-shaped refractive index change in transparent materials. Also, a

new type of optical sensor is proposed which relies on a complex helical shape of refractive index change.

Finally, Chapter six provides conclusions about this research and outlines possibilities for future work

Chapter 2: Background

2.1 Introduction

Glass is one of the most important materials in optics. It is a crucial material in a wide variety of applications. Nevertheless, it is challenging to micro-machine glass materials because glass is transparent for all visible wavelengths of light. Glass is unable to absorb energy carried by long-pulse lasers, which implies that the intensity of the incident laser beam stays below the threshold of machining effectiveness [26, 27]. Femtosecond lasers, however, are powerful tools for introducing microscopic modifications inside glass. The intensity of a given laser beam focal point exceeds the threshold for plasma formation when a femtosecond laser is involved in micromachining glass materials [28]. An optical cavity is created when plasma expands, since this plasma is confined inside the glass. It is possible to control space-selective induced structure inside the glass material when using the suitable conditions of ultrashort laser pulses. This chapter explores some of the basic nonlinear physics that explain how femtosecond laser pulses interact with transparent materials. Femtosecond laser pulses powered by only a modest level of energy can produce an extremely high peak power and intensity [29]. If the femtosecond laser pulses with high power and intensity come into an interaction, material response becomes highly nonlinear. The refraction index of the material changes responding to laser intensity and infrared energy is absorbed in transparent material while generating electrons [30]. This distinct characteristic of femtosecond laser technologies indicates enormous possibilities for micromachining transparent materials.

2.2 Non-linear propagation

In the nonlinear regime, when the laser intensity is low, the polarization is related to the electric field by

$$P = \varepsilon_0 + \lfloor \chi^1 E + \chi^2 EE + \chi^3 EEE + \cdots \ldots \rfloor = [\mathrm{P}^1 + \mathrm{P}^2 + \mathrm{P}^3 + \cdots] \quad (2.1)$$

where P is the induced polarization, ε_0 is the permittivity of free space, χ^n is the *n*-th order nonlinear susceptibility, and P^n is the n-th order nonlinear polarization. As depicted in Equation 2.1, all the perturbative nonlinear optics starts with induced polarization.

Each electric field of the right hand side of equation 2.1 can have different frequency components. The induced nonlinear polarization is the sum and/ or difference of these frequency components. Radiation is not necessarily observed at all of the frequency components at which there is a nonlinear polarization. The nonlinear polarization induced light generation and its propagations are governed by the following wave equation :

$$\nabla \times \nabla \times \mathrm{E}(\mathrm{r},\mathrm{t}) + \frac{1}{c^2}\frac{\partial^2}{\partial t^2} E(r,t) = \frac{-1}{\varepsilon_0 c^2}\frac{\partial^2}{\partial t^2} \quad (2.2)$$

where *E* is the electric field vector and *c* is the speed of light in a vacuum. For the radiation to be produced by nonlinear polarization, the nonlinear process must be phase-matched with the driving fields. Without phase matching, there is destructive interference between the radiations produced by nonlinear polarization at different positions in the material. As a result, special arrangements must be made to ensure a phase matched nonlinear process.

2.2.1 Refractive index change

The propagation of femtosecond laser pulses in amorphous materials such as glass is analyzed below. As the amorphous materials are isotropic, the tensor nature of the nonlinear susceptibilities can be dropped. All even-order terms in equation 2.1 can be cancelled since the amorphous materials have inverse symmetry. The following relations apply $\mathrm{P}^2 = \mathrm{P}^{-2}, E = -E$, but $\chi^1 = -\chi^1$ because the material has inverse symmetry. It can be written that:

$$-\mathrm{P}^2 = \varepsilon_0 \chi^2 (-E)(-E) = \mathrm{P}^2 \tag{2.3}$$

and $\mathrm{P}^2 = 0$, which implies that $\chi^2 = 0$. For the same reason, an equivalent argument holds true for the higher-order even terms of (2.1).

For an isotropic material and frequency dependency of the refractive index, the only processes that will be phase-matched are those, wherein all the fields have the same frequency, and therefore the same phase velocity. Consequently, ignoring the higher terms, polarization equation of (2.1) becomes

$$\mathrm{P} = \varepsilon_0 [\chi^1 + \tfrac{3}{4} \chi^3 |E|^2] E \tag{2.4}$$

and the refractive index can be expressed by

$$n = \sqrt{1 + \chi^1 + \tfrac{3}{4} \chi^3 |E|^2} \tag{2.5}$$

Considering the nonlinear term to be small (when compared to its linear susceptibility), and expressing the electric field strength in terms of laser intensity *I*, the refractive index can be written as:

$$n = n_0 + n_2 I \tag{2.6}$$

The laser intensity is given by

$$I = \frac{1}{2}\varepsilon_0 c n_0 |E|^2 \tag{2.7}$$

and the nonlinear refractive index is

$$n_2 = \frac{3\chi^3}{4\varepsilon_0 c n^2{}_0} \tag{2.8}$$

The nonlinear RI expressed in (2.8) boosts the self-focusing and self-phase modulation, and gives the propagation characteristics for short-pulse lasers when interacting with transparent materials.

2.2.2 Self-focusing

Spatial refractive index changes due to the spatial variation of intensity in laser pulses. Therefore, as (2.6) suggests, self-focusing takes place due to the intensity dependence of refractive index (RI). RI is higher at the center of the beam when compared to the outer beam area. This variation acts as a lens and focuses the beam as shown in Figure 2.1

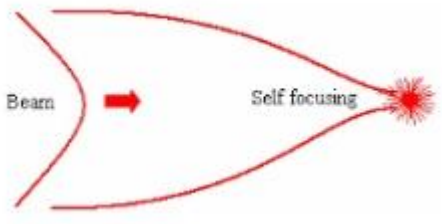

Figure 2.1: Schematic illustration of self-focusing. The spatial refractive index variation forms a virtual lens that focuses the beam

The strength of the self-focusing lens depends on the peak power of the laser pulse even though the refractive index variation depends on the laser intensity [31]. If the size of the incident laser beam is doubled, the laser intensity is reduced by a factor of four, which results in a reduction of the refractive index by a factor of four. As the size of the laser beam is doubled the area of the self-focusing lens is also increased by a factor of four. This increase in area compensates for the decrease in refractive index, giving the same output power.

An increase in the power of the laser pulse also makes self-focusing stronger until the power reaches a critical point. Degradation of laser beam quality occurs when the peak power of the laser pulses exceeds the critical power [31]. The critical power, P_{cr}, can be expressed as [32]

$$P_{cr} = \frac{3.77\lambda^2}{8\pi n_0 n_2} \tag{2.9}$$

where λ is the vacuum wavelength of the laser. In practice, other mechanisms halt the collapse of the beam due to its self-focusing. The intensity continues to rise and eventually becomes sufficient to non-linearly ionize the material when the laser beam is self-focused. Electron gas contributes to a negative refractive index (NRI) change, cancels the positive refractive index (PRI) change produced by the intensity dependant index, and prevents further self-focusing.

2.3 Nonlinear ionization

Micromachining of a purely transparent material is not possible through the linear absorption of incident laser light. However, the laser energy can be deposited inside the material through a nonlinear ionization process if the laser intensity is adequately high. In the following sections, two types of nonlinear excitation mechanisms are reviewed.

2.3.1 Nonlinear photoionization

The direct excitation of electrons by a laser field is called photoionization. Since transparent materials have a large energy band gap, a single photon of light does not have enough energy to lift an electron from the valance band to the conduction band. Hence, multiple photons must cooperate to excite an electron making up transparent material. There are two regimes of photoionization: tunneling ionization (TI) and multiphoton ionization (MPI), which depend on laser frequency and intensity [33].

In nonlinear photoionization (NPI), the tunneling process dominates when the laser beam has a strong field and low frequency. In this regime, the electric field of the laser is

stronger than the coulomb well that binds the valance electron to the parent atom [33]. As shown in Figure 2.2, a strong electric field can suppress the coulomb well, bound the electron tunnels through the short barrier, and becomes free.

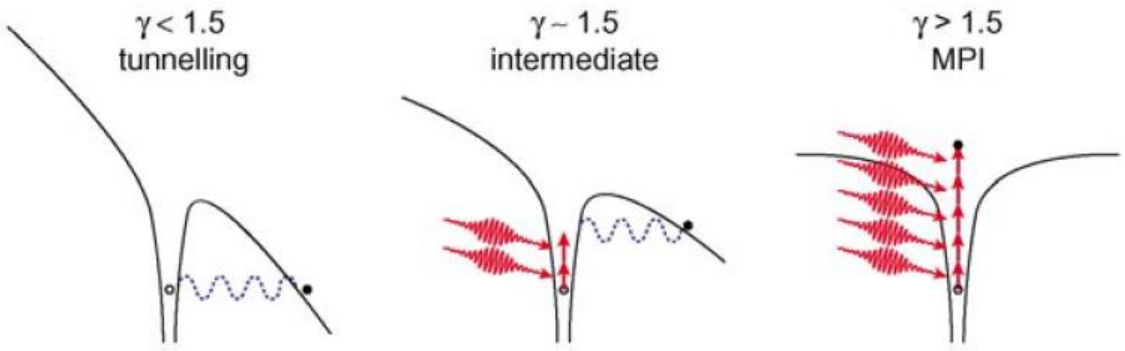

Figure 2.2 Schematic diagrams showing the photoionization process for different values of Keldysh parameter [33].

In the case of high frequency (not high enough that single photon absorption can occur), the tunneling effect is almost impossible. Therefore, NPI is usually described in terms of the simultaneous absorption of several photons by an electron as shown on the right in Figure 2.2. In order to transit from the valance band to the conduction band by multiphoton absorption, the electron must absorb enough photons. Both multiphoton absorption and tunneling can be described within the same framework, as suggested by Keldysh [34]. The transition from multiphoton to tunneling ionization is expressed by the Keldysh parameter γ as

$$\gamma = \frac{\omega}{e}\left[\frac{mcn\varepsilon_0 E_g}{I}\right]^{\frac{1}{2}} \tag{2.10}$$

where E_g is the band gap of the material, ε_0 is the permittivity of free space, n is the refractive index of the material, c is the velocity of the light, m and e are the reduced mass and charge of the electron, and ω is the laser frequency. When γ is much larger than 1, multiphoton ionization dominates the excitation process. In the intermediate regime, photoionization is a mixture between tunneling and multiphoton ionization.

2.3.2 Avalanche ionization

Free-carrier absorption followed by impact ionization is involved in avalanche ionization. As shown in Figure 2.3, a valance band electron of the material linearly absorbs several laser photons, and subsequently, moves to higher energy states in the conduction band. When the electron absorbs a photon, it must transfer momentum by absorbing or emitting a photon or by scattering off an impurity in order to conserve both energy and momentum [35]. Following the absorption of n photons where n is the smallest number that satisfies the relation ($nh\omega \geq E_g$), the electron energy exceeds the minimum conduction band by more than the band gap energy [36]. Such an electron can collision-ionize another electron from the valance band as shown on the right in Figure 2.3. As a result, there are two electrons in the minimum conduction band. Therefore, the electron density (N), in the conduction band continues to increase while the laser field persists. The conduction band density grows according to

$$\frac{dN}{dt} = \eta N \tag{2.11}$$

where η is the avalanche ionization rate [36].

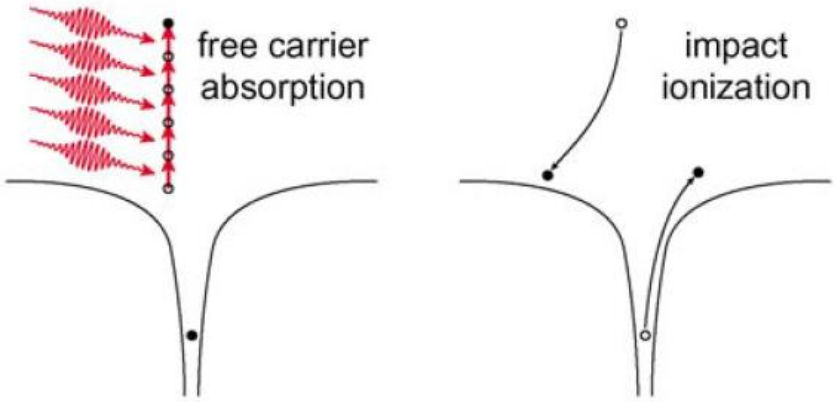

Figure 2.3 The avalanche ionization mechanism. A valance band electron linearly absorbs several photons through free carrier absorption and then starts impact ionizing another electron [33].

In order to start the avalanche ionization process, there must be some seed electrons existing in the valance band of the material. These initial electrons are provided either by a thermally excited carrier, by an easily ionized impurity, or by carriers that are directly photo-excited by MPI or TI.

2.4 Femtosecond laser assisted mechanisms

2.4.1 Plasma formation

In laser physics, plasma is typically an ionized gas that is considered a distinct state of matter. When intense femtosecond laser pulses interact with materials, free electrons are produced through ionization processes and the material enters this distinct state of matter, which is called plasma. The accumulation of free electric charges makes plasma electrically conductive. As a result, it responds strongly to electromagnetic fields.

2.4.2 Plasma defocusing

Plasma defocusing takes place due to the negative contribution of free electron to the refractive index. In plasma, the spatial distribution of electron density is maximum in the center and decreases gradually outwards. Therefore, a virtual negative lens is formed which is responsible for defocusing the ultrashort laser beam. Due to the balance between self-focusing, plasma defocusing and diffraction, femtosecond laser pulses can be transformed into self-trapped filamentation [37]. In this regime, the laser beam has a constant beam diameter even over a long distance [38]. By applying ultrashort laser beams, pulse energy can be efficiently utilized for the creation of long cavities in transparent materials consisting of filaments.

Chapter 3: Refractive index change using pulse filamentation

Local optical properties are changed when an ultrashort laser beam is focused inside a transparent dielectric material. Some researchers recently found that femtosecond pulses can inscribe modified structures inside transparent materials when the laser beam is tightly focused inside the material [39, 40]. Permanent refractive index change of single-mode fibers using ultra short pulses has also been reported [41]. Refractive index increases up to 0.035 induced by laser irradiation have been demonstrated in Ge-doped bulk silica glass [42]. Index modification of glass materials using ultra short pulse lasers has attracted attention for its potential to improve the fabrication of fiber optic devices. However, controlling the deposition of femtosecond pulse energy is important for photonic device fabrication using glass. The pulse filamentation induced by femtosecond lasers can enhance the guided delivery of the pulse energy for permanent refractive index changes in transparent materials [43]. This chapter provides a brief study on refractive index change in glass materials and introduces a simple lens fabrication that relies on controlling the beam pulse intensity using femtosecond laser pulse filamentation. Femtosecond laser direct writing provides a unique capability to change refractive index of transparent materials.

3.1 Introduction

Increasing the intensity of pulses confined to a range close to the laser focal volume continues to indicate amazing physical phenomena. Many researchers have reported interesting phenomenon such as pulse filamentation induced temporal reshaping and multiple foci in fused silica using intense femtosecond laser pulses [44-46]. Controlled ultrashort-pulse filamentation suggests great potential for applications such as optical devices and waveguides in transparent materials. Cutting glass plates using the filamentation of ultrashort laser pulses has been demonstrated [43]. In order to change the refractive index in transparent dielectric materials, uniform progress of the filament plasma column is employed for better control. In fact, for pulse filamentation, it is essential to control the size of a plasma column in a medium. The analytic estimation of filament length in air as a function of pulse duration and beam energy was demonstrated [38]. Balance between self-focusing and multiphoton ionization results in self-guided filament propagation in fused silica over several Rayleigh length [47]. Prolonged filament pulse propagation can be achieved by increasing the power density at focal point and minimizing losses. However, it is challenging to reach ultra-high -power density, because the light at a focal volume spreads longitudinally and radially. Increasing the peak power of laser pulses may lead to optical aberration. Pulse filamentation is a complicated phenomenon due to its nonlinear absorption and accompanying optical effects such as aberrations in transparent materials. Therefore, understanding the pulse filamentation phenomenon is crucial to produce controlled index change in transparent materials.

One dominating parameter required to form the appropriate filamentation length of the femtosecond laser in transparent materials is an intensity distribution at the focal point. In order to form the pulse filamentation, spaced plasma spots are formed regularly until the laser pulse peak power is higher than the critical power. The balance between alternative Kerr self-focusing and defocusing of self-generated plasma then continues along the propagation axis of the filament [48]. The pulse energy is subsequently consumed and weakens in ionizing the medium during filament propagation. Finally, self-focusing is collapsed by diffraction and plasma defocusing. Figure 3.1 shows the basic mechanism of ultrashort pulse filamentation.

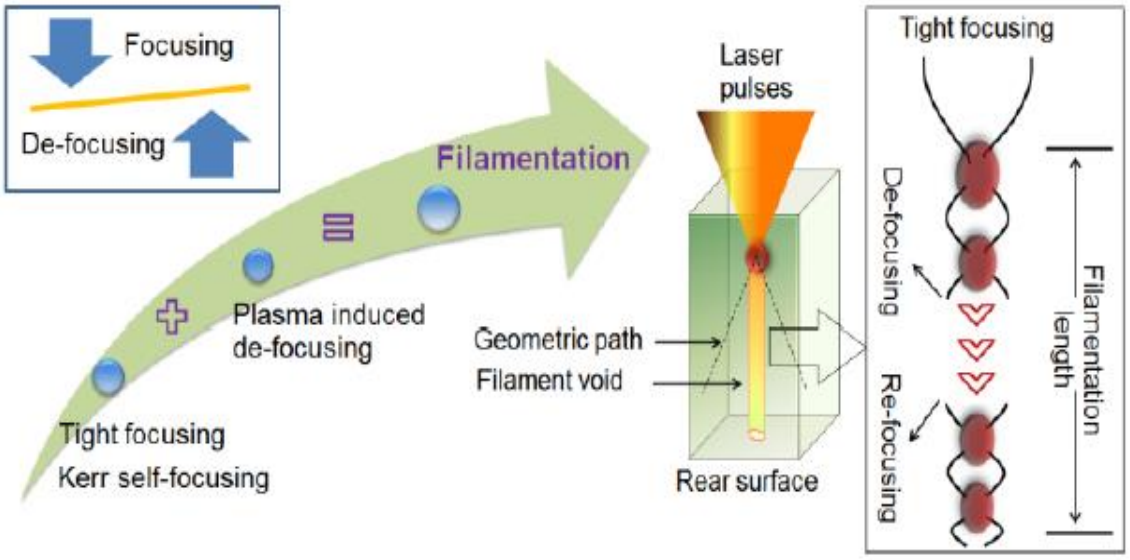

Figure 3.1. Filament propagation mechanism in transparent materials [49].

Previous work demonstrated that premature termination of filaments was promoted by an additional diffraction induced by plasma, even though the peak power was higher than the critical power [50]. Therefore, it can be assumed that the original plasma volume

when the beam is focused can be determined by the intensity distribution at focal point. This can also effect the size of the plasma spots and the length of filament. In order to retain extended length of filamentation, a glass plate was employed underneath the objective lens [43]. This study shows that the use of a glass plate can increase the effective numerical aperture (NA) and the density of the laser energy into a tiny focal volume, which results in a narrow and long filament ionization column inside glass materials. Figure 3.2 shows the high density pulse energy for small and long filament propagation.

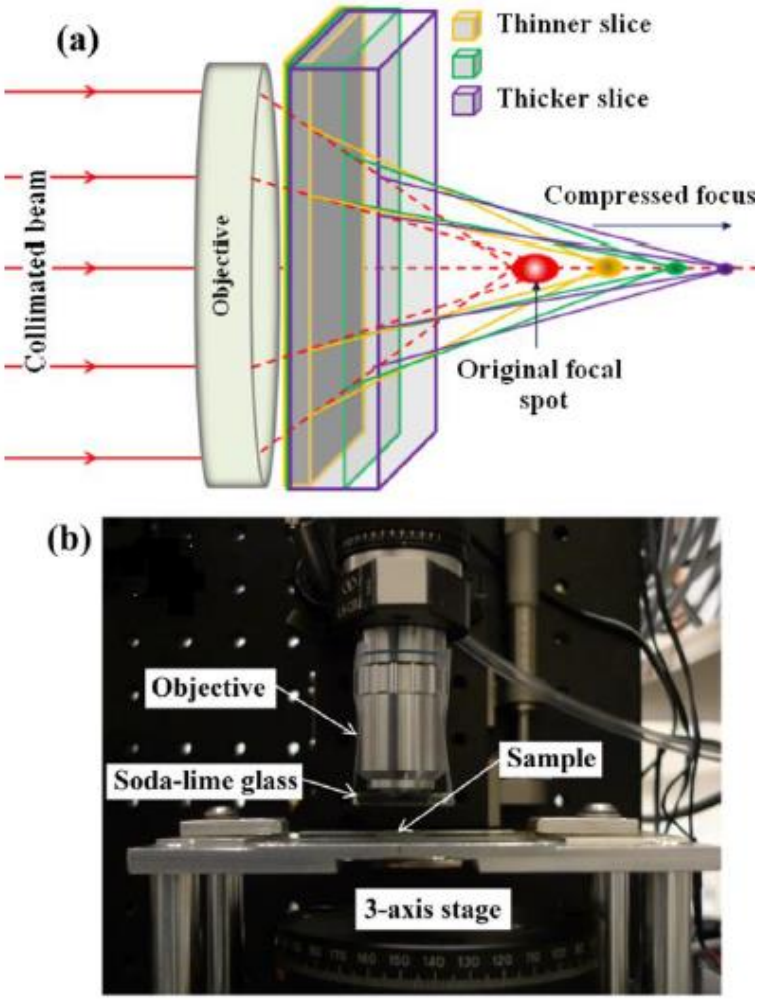

Figure 3.2 (a) Glass plate as a compressor of laser beam before the beam is irradiated into the sample, (b) picture of laser setup assembly for filament fabrication [43]

In this chapter, laser pulse filamentation produced through variable pulse energy will be demonstrated. Furthermore, a gradient index lens for pulse filaments is proposed as a promising approach for femtosecond laser direct writing.

3.2 Experimental setup

A schematic diagram of the femtosecond laser system is shown in Figure 3.3. Femtosecond laser (Spectra-Physic ultrafast Ti: Sapphire laser) with a 120 femtosecond pulse width and 1 KHz repetition rate at a central wavelength of 800 nm was used for refractive index modification of a fiber. The laser beam was guided into a 50X objective lens (Numerical aperture: 0.55) and focused on to the core of the transparent material. An electronic shutter controlled by computer was used to control the transmitted laser beam at the desired focal position of the fiber. The effect of refractive index modification that occurs during irradiation of femtosecond pulses was observed through a CCD camera installed above a dichroic mirror. Figure 3.3 illustrates the femtosecond laser system.

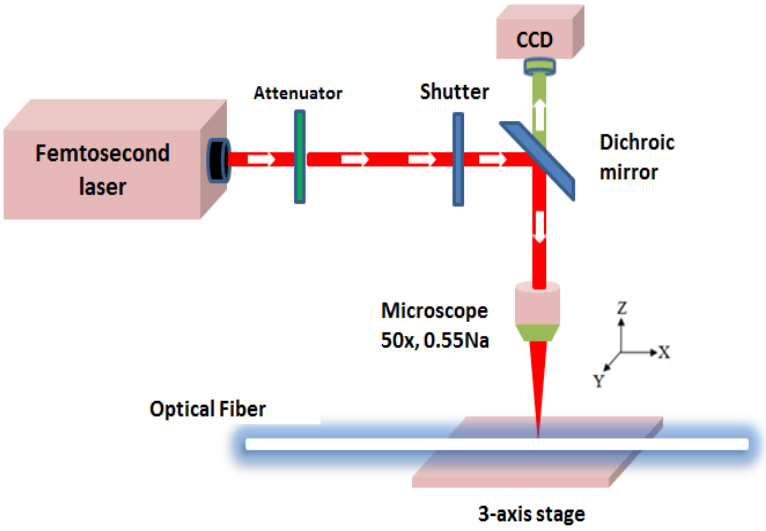

Figure 3.3. Schematic of the femtosecond laser system for refractive index change using pulse filaments

3.3 Result and discussion

3.3.1 Filament by different pulse energy

With the laser specifications indicated above, pulse filaments were applied to a commercial soda-lime glass with different pulse energy so as to verify the possibility of refractive index change in transparent materials. Figure 3.4 shows the pulse filament propagation versus pulse energy.

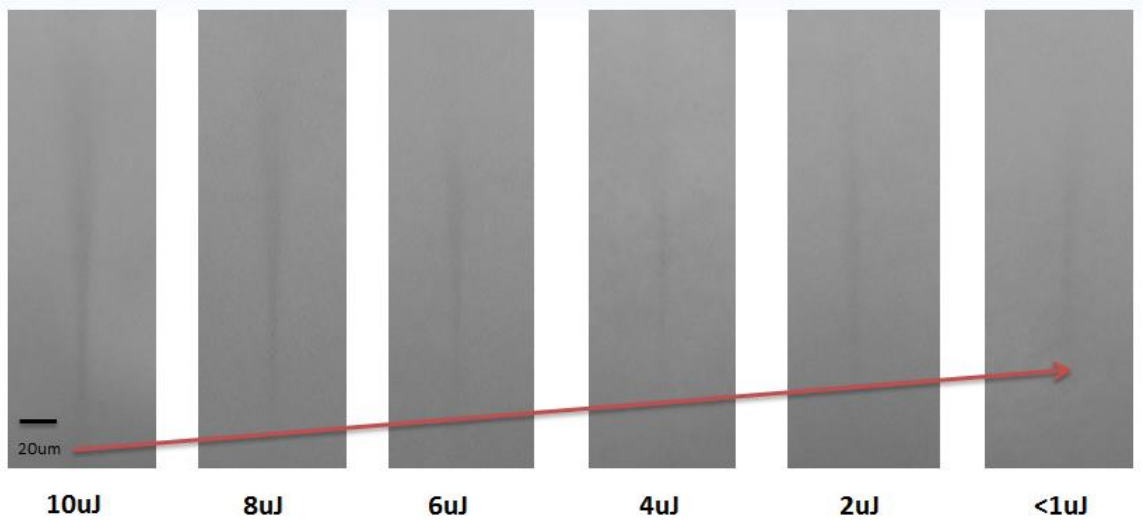

Figure 3.4 Cross section of pulse filament propagation for different pulse energy in a soda-lime glass

The measured lengths of filaments were approximately 180 µm, 170 µm, 150 µm, 140 µm, 130 µm, and 120 µm with laser pulse energies were from 10 µJ to 1 µJ, respectively. It is very important to achieve pulse filamentation without damage in the transparent material since applications such as fiber grating sensors require high precision

measurements. The damage in transparent mediums may result in loss of light intensity or inducing signal noise in the optical sensors. Damage to the soda-lime glass was observed after increasing the pulse energy over 10 µJ. Figure 3.5 displays the cross section of the soda-lime glass damaged by femtosecond laser pulse.

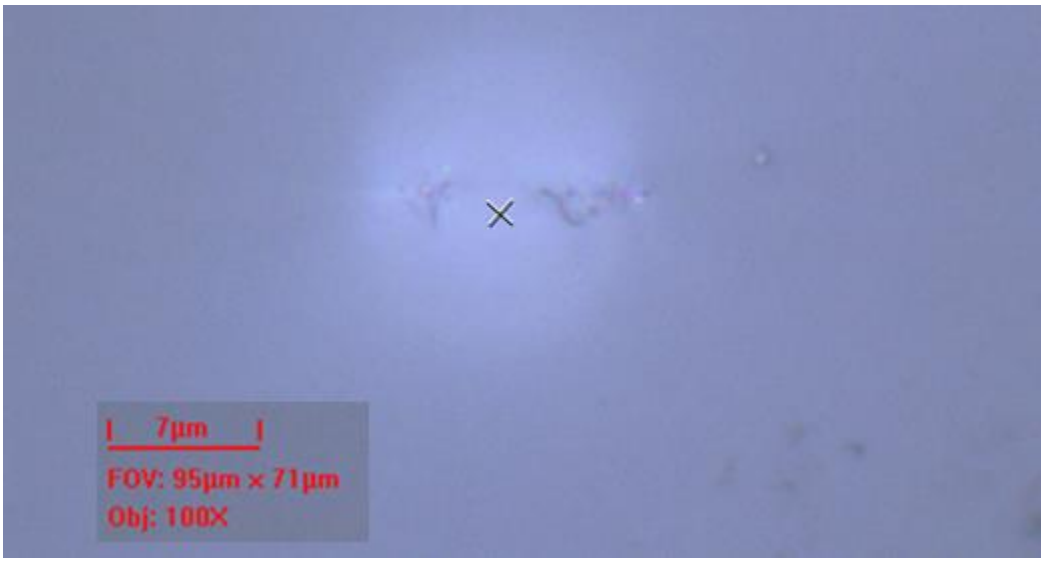

Figure 3.5 Cross section of the damaged glass by femtosecond laser pulse

In order to investigate the effect of this damage, refractive index change with and without damage using the pulse filament were implemented in two single-mode optical fibers and then they were connected to a broad band light source (AFC BBS-1550), which transmits light into the fiber core. A spectrum analyzer (PHOTONETICS Walics) was used to show the intensity of transmitted light at various wavelengths. Figure 3.6 shows the loss of light intensity and the generated noise because of the damage inside the single mode optical fiber.

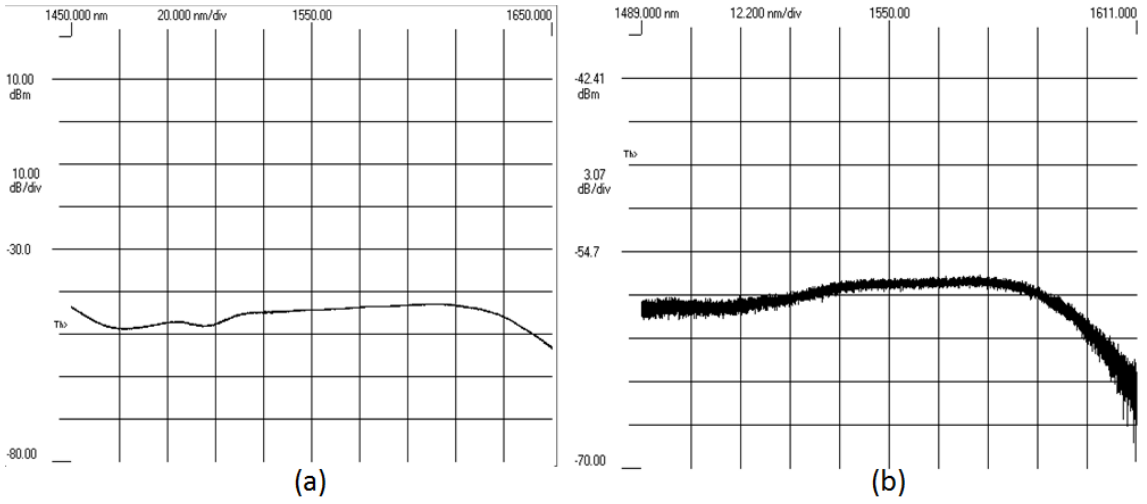

Figure 3.6 Transmission spectrum of the single mode optical fiber. (a) refractive index change without damage (b) refractive index change with damage by laser pulses

The measured light intensity of the optical fiber without damage at 1550 nm was -45 dB and the noise was relatively small. In contrast, the light intensity of the optical fiber with damage by laser pulse was -57 dB while significant noise was observed compared to the first sample. Damage due to the refractive index change, such as micro-cracks, decreases the productivity of optical fiber sensors and reduces precision of fabrication. Therefore, an efficient refractive index modification induced by pulse filamentation is essential for optical devices. Considering the findings of this pulse filament propagation experiment, a new idea of gradient lens fabrication emerges, as will be introduced in the next section.

3.3.2 A concept of gradient index lens fabrication using pulse filamentation

Gradient index (GRIN) lens is an optical component produced by gradient refractive index change. GRIN lens fabrication has the following two advantages. It can be assembled with flat surfaces and does not have any aberrations. Various methods for fabricating of GRIN using infrared transmitting glass lenses have been reported including ion exchange, chemical vapor deposition, sol-gel processing, copolymer diffusion, layered diffusion and molded fusion [51-54]. The most well-known and successful technique for GRIN lens fabrication is an ion exchange method. Ion exchange uses the exchange of single valent ion existing in molten salt baths (dopant ions) and single valent ions in glass (host ions). Since there is a concentration gradient across the border of molten salt bath and the glass sample, ion inter-diffusion occurs. Figure 3.7 depicts the GRIN lens fabrication method using ion exchange.

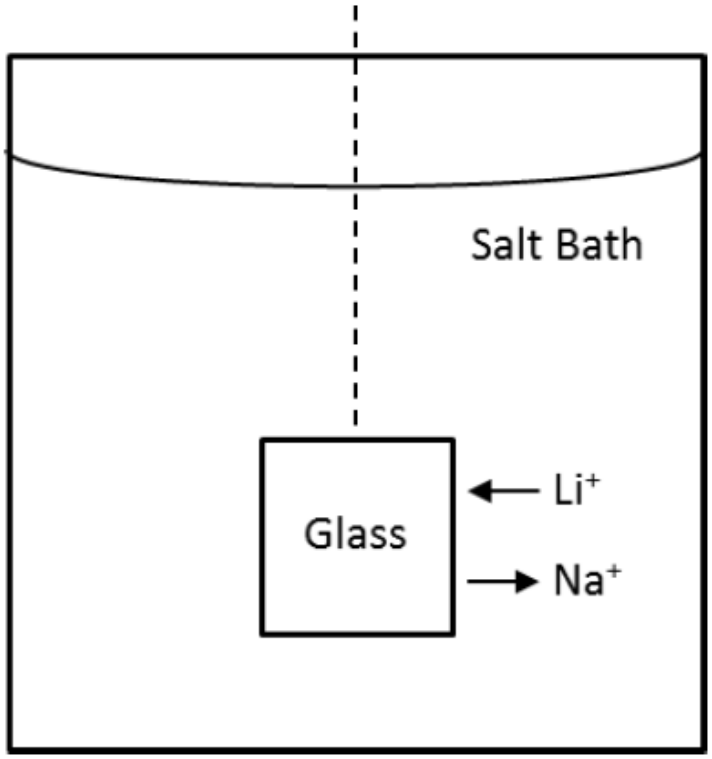

Figure 3.7 A typical ion exchange experiment. Lithium ions in the glass exchange for sodium ions in the salt bath [55].

It should be noted that fabrication of GRIN lens using various methods mentioned above is still challenging. Fabrication of large diameter of GRIN lenses using ion exchange is limited by long diffusion time. They require additional materials such as a liquid melt with lithium ions for fabrication. In order to overcome these limitations, a new concept of GRIN lens fabrication method using laser pulse filamentation is introduced in this thesis. Radical gradient index lens was fabricated with the idea that pulse filament can change the refractive index of glass materials, and that the focal point in glass materials can vary. Figure 3.8 illustrates GRIN lens fabrication.

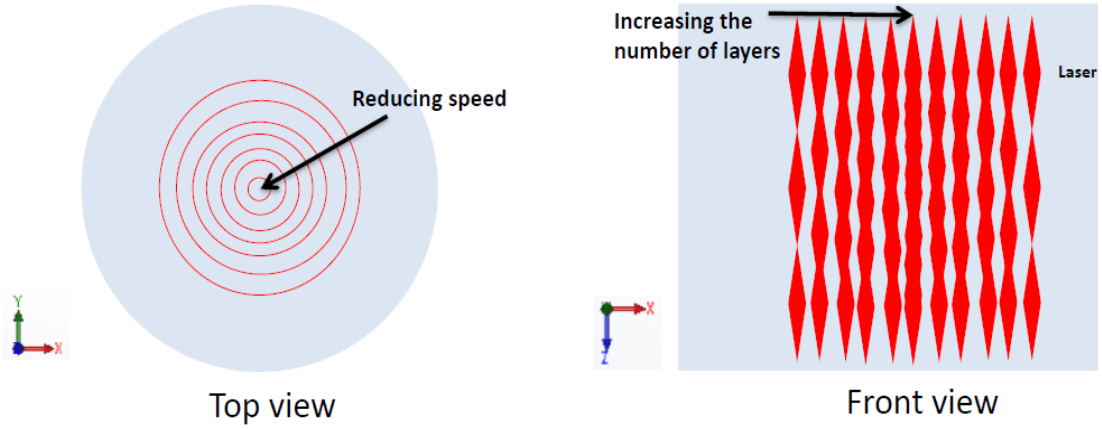

Figure 3.8 Schematic of GRIN lens fabrication. Laser scanning speed decreases and the number of scanning layers increase as it goes to the center

Laser scanning speed was decreased from the side to the center of glass samples, resulting in greater overlap between filaments induced by femtosecond laser. Further, the number of laser scanning layers were increased in the Z-axis, which means an increasingly greater number of filaments were observed to overlap when moving from the edge to the center. This can result in higher refractive index change at the center point than around edge. Figure 3.9 shows the profile of laser beam intensity with and without modified refractive index of glass plates.

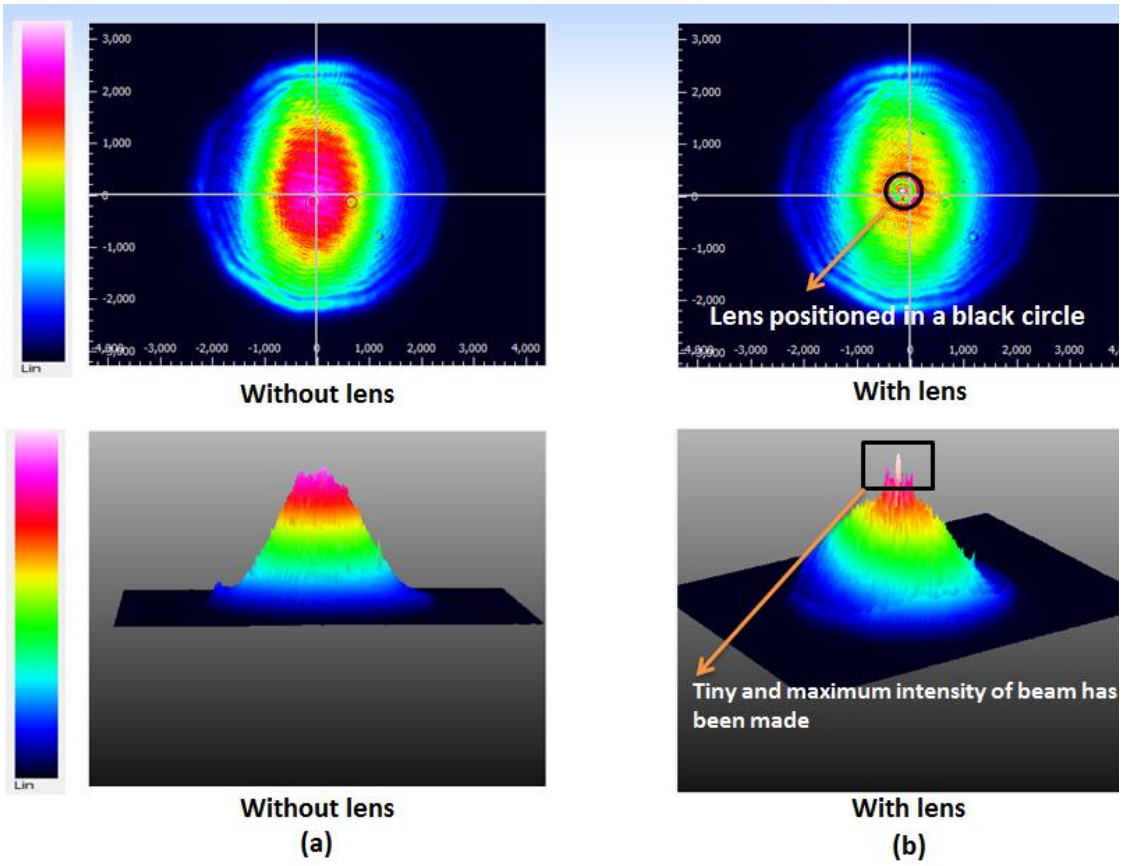

Figure 3.9 Profile of laser beam intensity. (a) without GRIN lens (b) GRIN lens placed on the beam profiler

After fabrication of GRIN lens using femtosecond laser induced filaments, the lens was positioned underneath the laser beam to verify its gradient index. Figure 3.9 (a) shows the Gaussian distribution of the original laser beam. There is no peak point in this instance, since there was no lens or other substrate placed on the beam profiler. However, in Figure 3.9 (b), beam intensity increases to the edge of the lens, and rapidly reduces at the starting point of the lens. Afterwards, the beam intensity significantly rises to the peak

point. This means that the light was focused by the fabricated GRIN lens and gradually increased refractive index from edge to the center of the glass sample was produced by the femtosecond laser induced pulse filaments. Figure 3.10 shows the X-Y profiles of the light intensity.

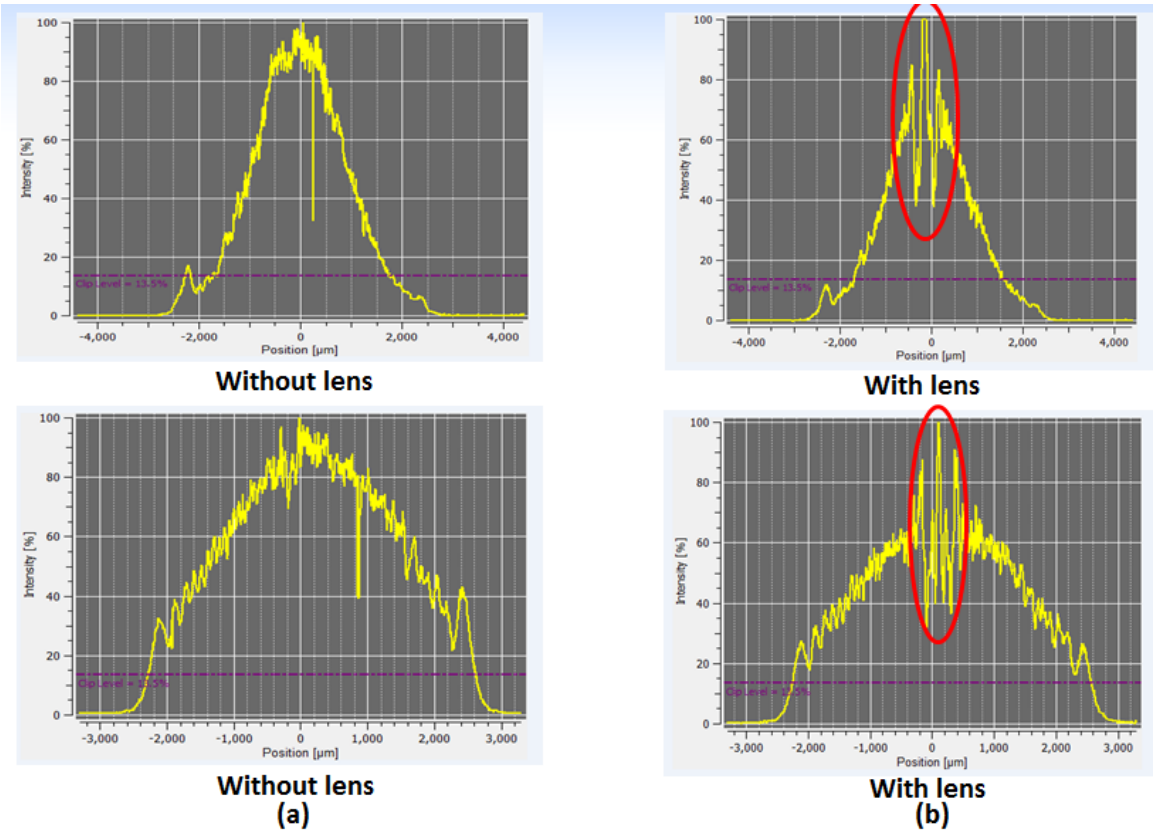

Figure 3.10 X-Y beam profile. (a) without lens, there is no light focused (b) light intensity rapidly decreases at the lens placed and focused sharply.

As an emergent technology, GRIN lens fabricated by femtosecond laser pulse filamentation still lacks precision since it is challenge to control uniform refractive index change. Even so, at this early stage it already proves the viable fabrication of commercial productions with attendant advantages such as simplistic method and relatively short fabrication time.

3.4 Conclusion

The experimental study of femtosecond ultrashort pulse induced filamentation was demonstrated using femtosecond laser system in this chapter. It was verified that the length of filaments are effected by pulse energy and that the length of filaments increased as the pulse energy rose. In order to manipulate this filament for optical device production, refractive index change with damage in the glass material such as cracks was intentionally produced. As expected, damage inside the single-mode optical fiber produced a loss of light intensity and noise as shown by the optical spectrum analyzer. For use of the ultrashort pulse filament in other optical application devices, the new concept of GRIN lens fabrication technique was developed. Gradually increased refractive index produced by different laser scanning speeds and pulse overlapping rates made light more focused, as shown by the beam profiler. I believe that the proposed technique has potential to replace existing methods of GRIN lens fabrication with the advantages such as simplified process by laser direct writing and fabrication time.

Chapter 4: Glass welding using ultrashort pulse filamentation

4.1 Introduction

Joining transparent materials using ultrafast pulse laser, whether glass to glass or glass to silicon, has been investigated by many researchers [56], since it has clear advantages compared to welding by conventional laser with continuous wave function. Ultrafast pulse laser welding enables highly accurate selection of the welding region, due to very short heat-diffusion time and because it does not involve additional adhesive substances that deteriorate the functionality of joined materials [20]. Moreover, joint strength of materials welded together by ultrashort pulse laser is comparable to inherent strength of materials prior to welding. For these reasons, the bonding method for transparent materials by pulse laser, which maintains mechanical, thermal, and chemical properties of original materials, has been employed in a variety of applications. These include micro-fluidic devices, sensors, and optical devices [57]. As the same adhesive-free joining methods, direct bonding by Van der Waals force has been widely used for proper joining [58]. However, this method may be vulnerable to external effects such as thermal and pressure changes. Therefore, it is not considered ideal for joining process meant to result in durable products. In addition, some mechanical properties such as low surface flatness and roughness are required in order to achieve direct bonding [59-61]. In order to achieve proper conditions for direct bonding, materials may need post-processing such as precise polishing and cleaning processes which means a rise in the cost of materials, and it is a challenge to obtain optical contact on an entire area of material surface. Therefore,

ultrashort laser welding methods have been investigated by researchers who seek to overcome the constraints of present direct bonding practices. Kongsuwan et al. investigated the morphology of welded cross-sections and analyzed the relationships between welding widths and absorption widths as well as changes in mechanical properties using BK7 glass plates [62]. Horn et al. demonstrated joining geometry and joint strength of the welding seam in high repetition rate laser irradiation using borosilicate glass [63]. Richter, investigated conditions of the laser burst regime and tested repetition rates to optimize breaking resistance of fused silica. They determined stress levels induced by laser pulses generally relies on laser power [64]. Fabrice et al. conducted a study of welding of dissimilar transparent materials such as borosilicate glass-fused silica and silicon-borosilicate glass using femtosecond laser with both high and low repetition rates [56]. Also, translation velocity and parameters resulting in joining by varying the laser pulse energy have been investigated [65-68]. However, these past studies mainly focused on laser parameters and joint strength in a small welding area (from 100 μm^2 to 10 mm^2) and they used high-quality glasses such as fused silica and BK7, which have better smoothness and flatness than normal soda-lime glasses or microscope slides. The choice of materials in previous lab studies leads to a rise in experiment costs and limits the applications of results to small devices.

In the present study, joining normal microscope-slide glasses using femtosecond laser has been performed to verify the possibility of welding both wide and targeted regions. Experiments in this thesis used forcibly achieved optical contact by a fixture in order to

show that this welding method can be feasibly used for real-world applications, such as micro-fluidic channel assembly.

4.2 Principle of ultrashort-pulsed laser welding

Two different methods of the laser welding are advocated in this thesis: low repetition pulse rate, and high repetition pulse rate). The difference between them depends on how long it takes for the pulse period to heat the focal volume. Material melting is produced by a single pulse in the low-repetition rate regime. By contrast, the material molten zone is reached because of the cumulative effect of heating in the high-repetition rate regime. Figure 4.1 shows the principle of the laser micro welding technique.

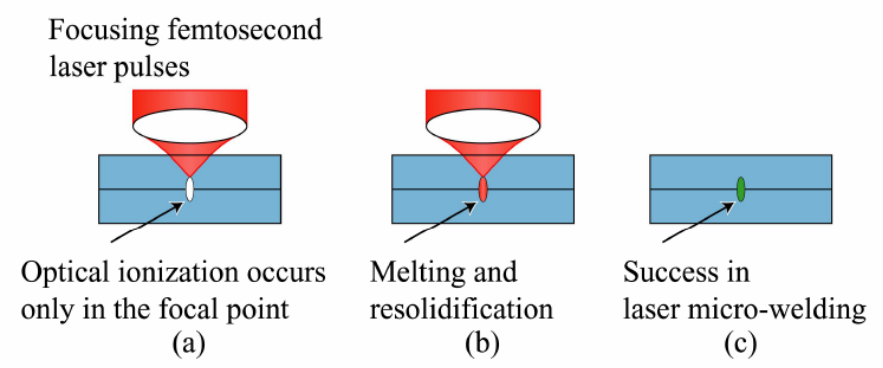

Figure 4.1 Schematic diagram of the laser welding process. (a) Nonlinear ionization occurs at interface of two substrates. (b) creation of localized plasma in the focal volume. (c) resolidification of material results in micro-welding [69].

A filament melts both transparent materials when ultrashort laser pulses are tightly focused at the interface of the materials. The intensity in the filament is high enough to initiate nonlinear absorption volume by field ionization processes, such as multiphoton ionization, tunneling ionization and avalanche ionization. This nonlinear absorption creates an electron-ion plasma localized in the focal volume. Subsequently, a glass-melting zone occurs between the two transparent materials and around the focal volume. Finally, two sample materials are joined through re-solidification [70].

There are certain advantages to femtosecond laser micro-welding. For instance, the welding of transparent materials can be achieved through direct irradiation of a laser beam without intermediate layers. Moreover, femtosecond laser welding allows space-selective joining that results in reducing residual thermomechanical stress since the melting zone of the materials is limited around the focal spot. In addition, it is possible to join dissimilar materials if one is transparent.

4.3 Experiment setup and fabrication

Experiments have been carried out using a commercialized, mode-locked fiber laser manufactured by PolarOnyx. Inc. The laser output beam used in this experiment is Gaussian shape, and it has a pulse duration of 700 fs and a spectral bandwidth centered at 1030 nm. The pulse repetition rate was fixed at 99.6 kHz and the average output power was 1.1 W. An electronic shutter controlled by computer was used to turn on and off the laser beam, targeted for irradiation at a desired spot within the interface of the sample

materials. The laser beam was focused by an objective lens (numerical aperture: 0.42) into the interface of the sample. The live images capturing focused irradiation of femtosecond pulses were observed through a charge-coupled device (CCD) camera mounted above a dichroic mirror. Two commercial microscope glass slides (borosilicate) were cleaned with acetone in order to remove impurities that make a gap between the samples before being placed within the fixture. The sample was put on a computer-controlled 4-axis stage to achieve perfect alignment along the laser scanning path. The commercial software, GOL3D was used to create the laser scanning path. The laser system for glass welding is shown in Figure 4.2.

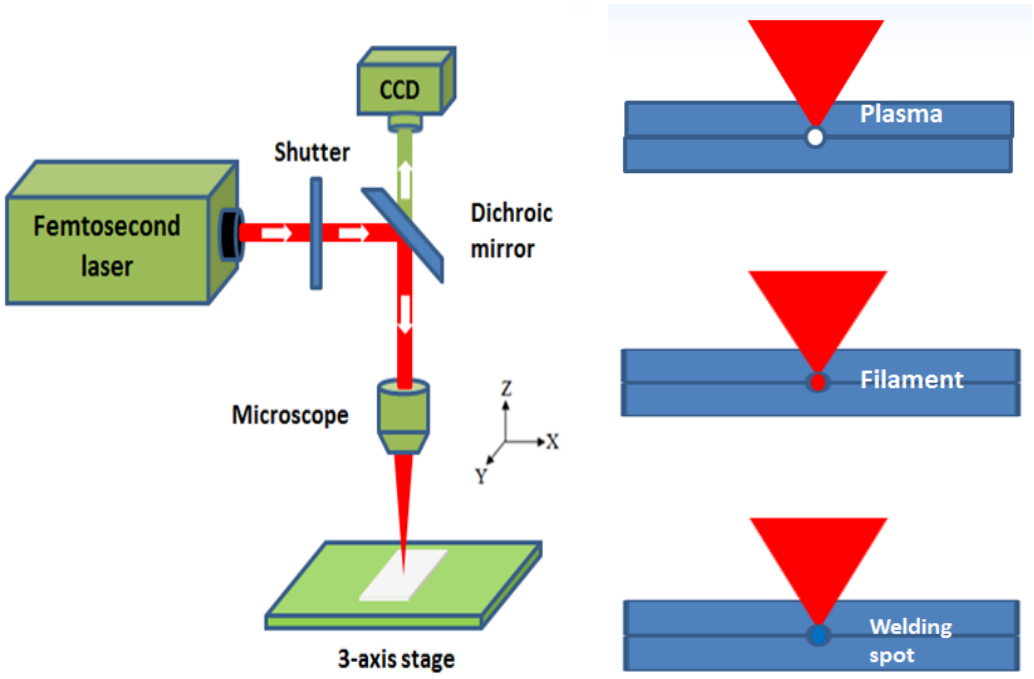

Figure 4.2. Schematic of the experimental setup for glass welding.

Optical contact of two transparent materials is very important for glass welding. Sample materials should have sufficient smothness and flatness (5 nm roughness and λ/2 flatness) to obtain optical contact. Note that these condition requirements may increase manufacturing costs because it needs high quality materials such as BK7 and fused silica. In addition, optical contact cannot be achieved on entire surface of the sample even if the high quality materials are used. Therefore, for purposes of the present study, a customized fixture was fabricated to obtain a wide area of optical contact. Figure 4.3 shows a schematic of the created fixture for wide optical contact area:

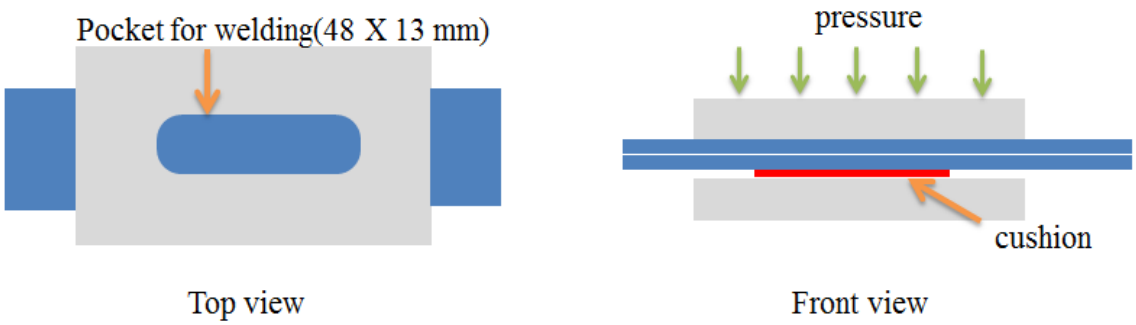

Figure 4.3. Schematic of customized fixture for optical contact of the sample using pressure

Two transparent material substrates are stacked together on the cushion. The moderate pressure is applied to the sample, which is created when the aluminium fixture is clipped together. This pressure applies to the top and bottom plates and achieves optical contact at the interface of the sample. The laser beam was irradiated through an open pocket to the interface of the sample materials. Using this type of cushion achieves uniform pressure for optical contact and possibly aids in widening welding areas. It also prevents

over-stressing and fracturing of the sample. Experiments showed that the cushion area must be smaller than the pocket area, otherwise interference patterns result: indicating a gap between the sample layers. The stacked sample moves together with the 4-axis controlled stage, while the focused laser beam is irradiated to the sample.

4.4 Result and discussion

4.4.1 Glass welding by different air gaps

The focused laser beam was irradiated at the interface between the two microscope slides for femtosecond laser welding. Since complete optical contact of the entire welding area cannot be achieved even though the customised fixture is used for laser welding, several times laser welding was conducted at the sample interface with different air gaps in order to verify how big gaps between glasses allow laser welding. Different interference colours were obtained by applying various pressures to the glass slide sample. According to thin film interference theory, a dark band appears where the glass slides tightly touch together forming the optical contact. The interference colour at the point of a gap changes from violet to red as the distance between the slides increases. Figure 4.4 shows the color bands produced by thin film interference in the air between two glass slides.

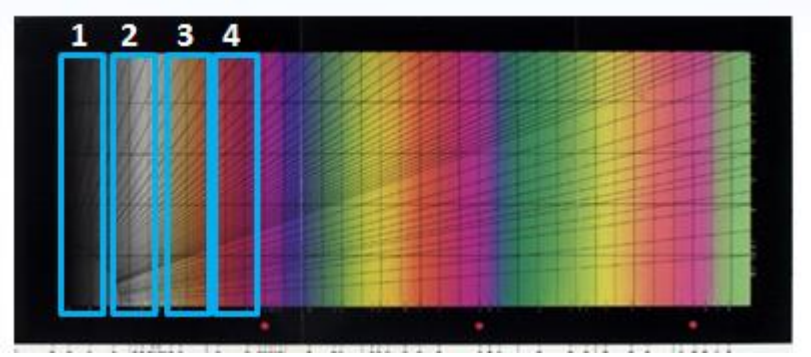

Figure 4.4. Colour bands by thin film interference. The colour changes from the left to right as the gap increases.

Experimental results show that the laser welding conducted in the black and white bands (areas 1 and 2 in Figure 4.4) successfully joined the two glass slides. There were no traces of micro-cracks or machining debris following the experiment, as shown in Figure 4.5.

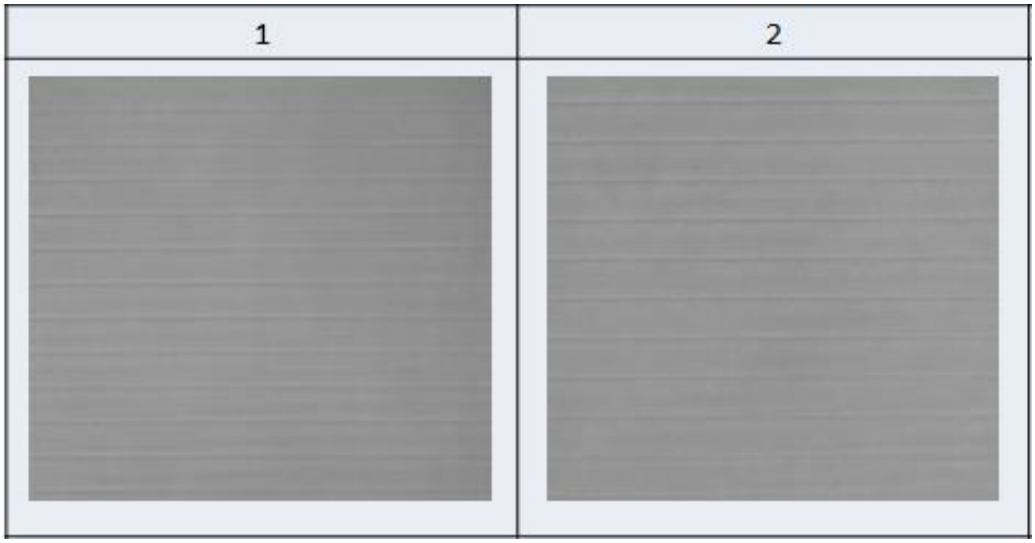

Figure 4.5. Microscope images of welding seam conducted in the black and white band area (area 1 & 2 in Figure 4.4) at the interface of the sample two samples with different gaps were completely joined and no micro cracks were observed.

The thin, dark lines visible in the Figure 4.5 are welding seams inside the sample materials, and there was no variability in the shapes of welding seams in either areas. In contrast, micro-cracks or machining debris were observed in the welding areas that fell into the yellow interference colour band. It was assumed that the laser beam machined the glass substrate since the gap between the samples was too big for the laser welding. Another possibility is that micro-cracks could have been generated after the glass melting stage, because the force pulling glass surface back to its original position exceeded the strength of the welding seams. In the area of violet color band, the materials were completely machined by the laser beam without pushing materials into their meting zones.

Figure 4.6 shows microscope images of the machining areas of yellow and violet color bands.

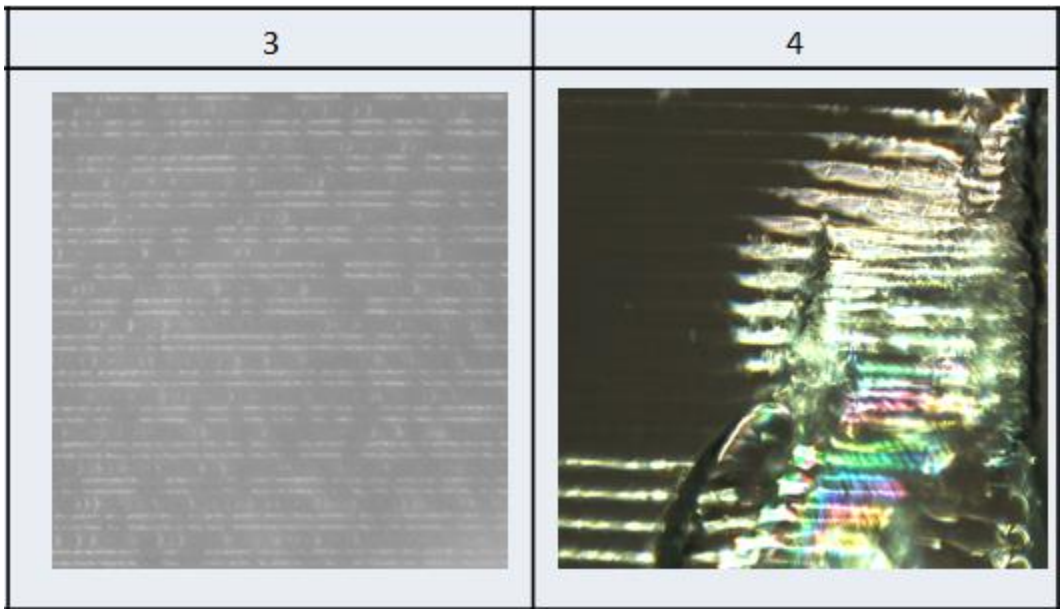

Figure 4.6. Microscope images of welding areas in yellow and violet color bands (area 3 & 4 in Figure 4.4). The welding sample conducted in the yellow color band has micro cracks and the laser beam ablated (not welding) the glass in the violet color band.

Shear strength tests were carried out after femtosecond welding in order to estimate the joint strength of the fused materials. The first sample was bonded by direct boding method using Van der Waals force, and the second sample was joined by femtosecond welding. As shown in Figure 4.7, a simple tensile tester able to measure maximum 10 N force was used for the test. The top and bottom pieces of the sample were fixed to the base of the tester.

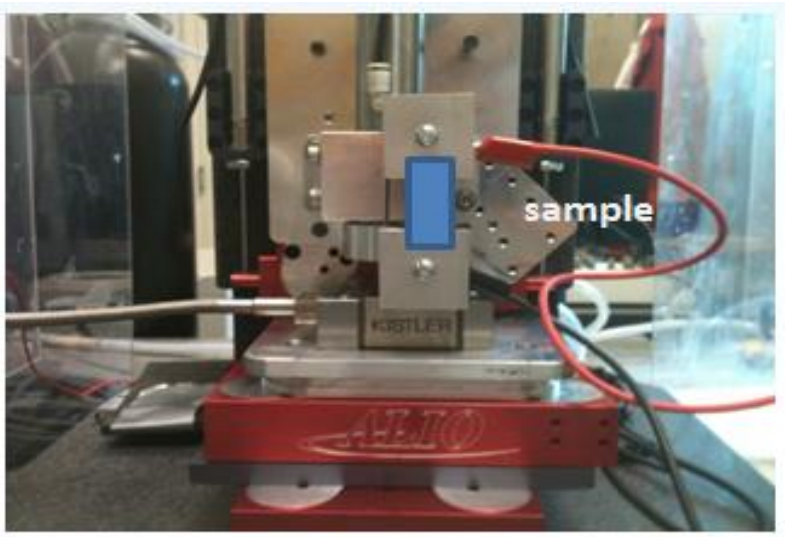

Figure 4.7. Picture of the tensile tester for joint strength. The sample was fixed in place through bolting.

The load was subsequently increased until the bonded samples were cleaved into two pieces. The joint strength was determined by dividing the pressure of the load by the surface of the bonding areas (measured at the point when the sample was cleaved). The fraction of the sample joined by direct bonding occurred at 3 Newton, meaning that the bonded sample was broken by that force. In contrast, the welding sample fused through femtosecond laser beam withstood until a force of 10 Newton, the maximum force of the tester. Therefore, the measured shear strengths of the two samples were 0.4 KPa and 50 MPa (at least), respectively. Figure 4.8 shows the sample strength test results.

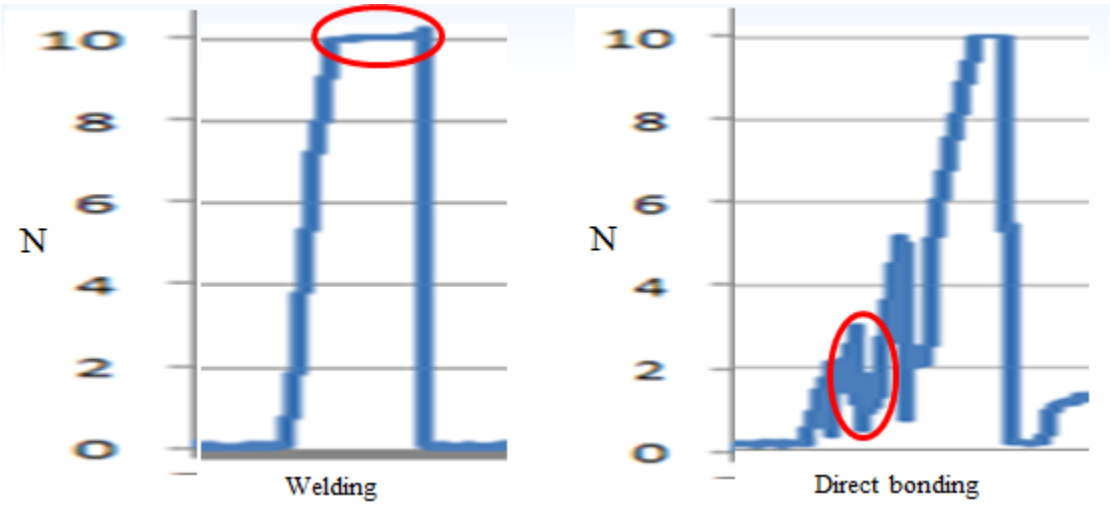

Figure 4.8 Shear test results. Welding sample was broken at 10 N (maximum force of the tester) and the sample joined by direct bonding was cleaved at 3 N.

4.4.2 Sealing of wide welding area

For various applications, such as manufacturing microfluidic devices, the femtosecond laser welding technique can effectively replace the current intermediate adhesive-layer used to seal a complete region and to protect the center region by using four-edge multi line welding [25]. Two commercial microscope slides without optical coating were used to show the viability of femtosecond laser welding. Figure 4.9 shows a welding sample effected by interference fringe inside of the welding lines. The total sealing area of the sample (produced by femtosecond welding) is 44 mm x 9.5 mm, which is much wider area than previous welding results which have been viably produced. This wide sealing area is achieved by a customized fixture creating optical contact over the sample surface.

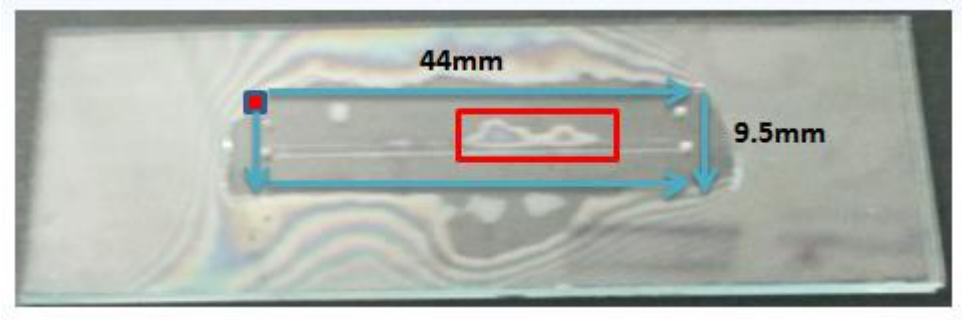

Figure 4.9 Camera view of four-edge sealing of glass sample by femtosecond welding. The interference fringe exists inside welding boundary.

In order to verify that the sealed area is completely isolated by the welding lines, the welding sample was submerged in water. Figure 4.10 shows that the center square region is well sealed by femtosecond laser welding. The interference fringe outside of the welding lines was almost completely removed after the water submersion test. In contrast, the interference fringe inside the welding area was not removed, meaning that water was not able to penetrate into the sealed area, since that area was completely blocked by the surrounding welding seams. This shows not only isolation from liquids but also that the materials were perfectly sealed against gases.

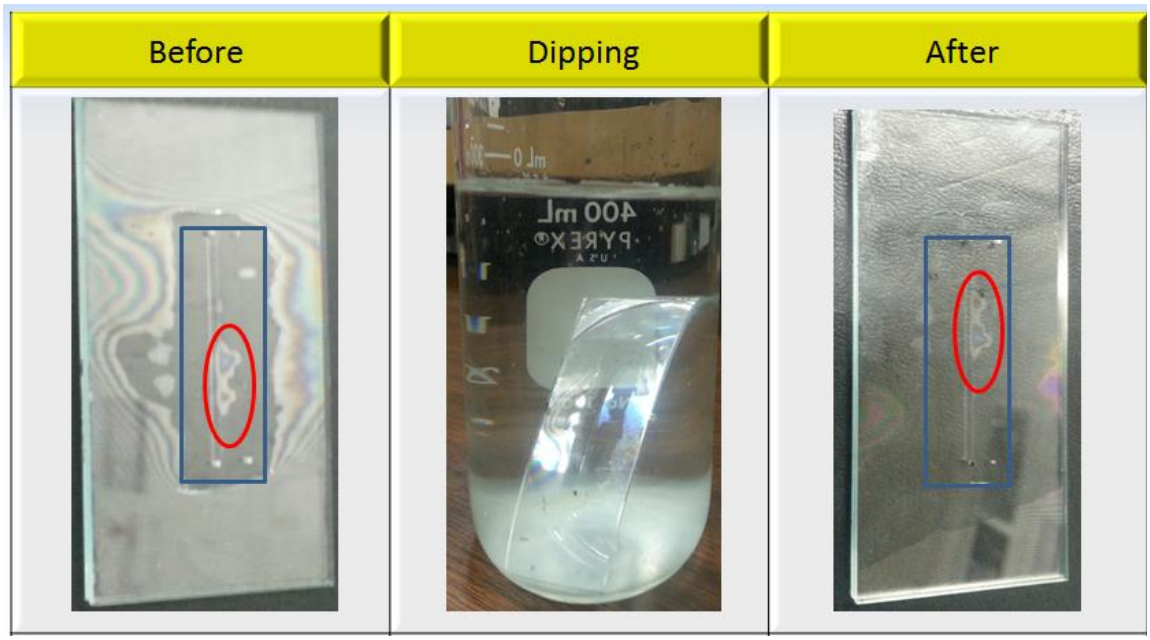

Figure 4.10 Water immersion test. The interference fringe still exists after the test.

In order to verify the viability of using femtosecond laser welding to produce micro-fluidic devices and to double-check that regions inside welding lines are completely sealed, a simple microfluidic sample was fabricated using a femtosecond laser. Figure 4.11 illustrates the microfluidic channel assembly fabricated by femtosecond laser machining and welding. First, a simple channel (0.5 mm width, 10 mm length) was machined on the top surface of the bottom glass slide and then 2 holes were machined on the top surface of the upper glass-slide and bottom surface of the lower glass-slide to insert liquid into the channel. The pulse width, wavelength, repetition rate, average power, scanning speed, and objective lens for machining the channel and the holes were 120 fs, 800 nm, 1 kHz, 0.4 W, 0.3 mm/sec and 20 X, respectively. The two glass slides with

channels and the holes were cleaned using acetone and then welded using the same procedure explained above.

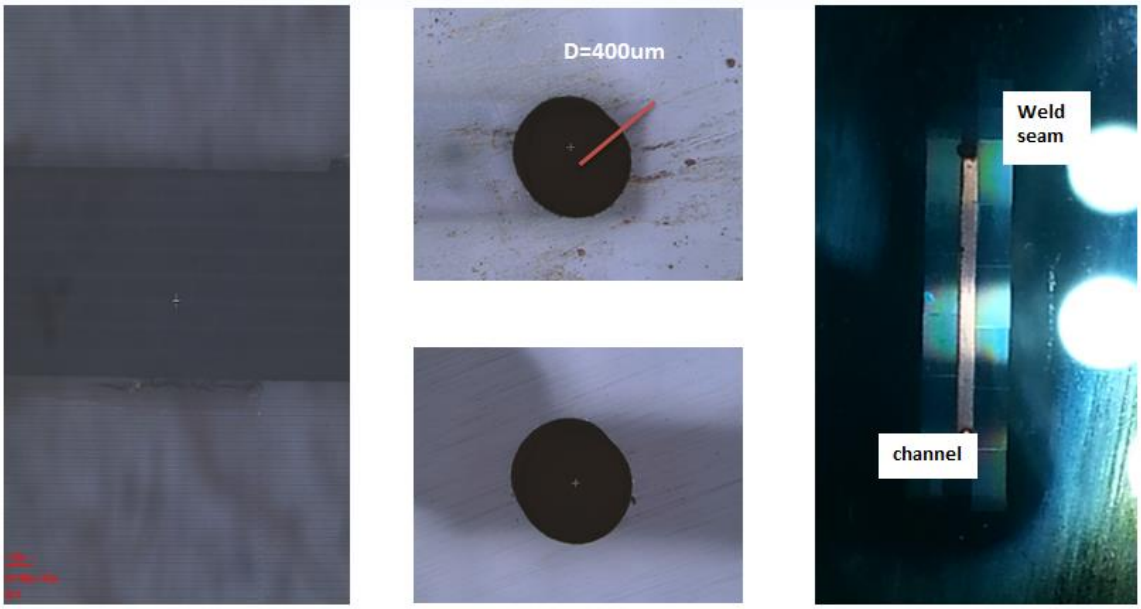

Figure 4.11 Microfluidic channel assembly fabricated by femtosecond laser machining and welding.

After fabrication of the microfluidic channel assembly, a solution insertion test was conducted using red ink. Then the sample was illuminated by an LED backlight to verify the integrity of the welding seam by checking for leakage from the channel. As shown in Figure 4.11, no ink leakage from the channel was detected. Red ink inserted through the hole at the top surface of the sample flowed into the channel and then slipped out through the hole in the bottom surface of the sample. The welding seams around the channel were clearly seen to have withstood the experiment without debris or cracks.

4.5 Conclusion

Glass welding using femtosecond laser was demonstrated as a viable procedure. A customized fixture to secure a wide region of optical contact was adopted. Welding according to different air gaps between two glass substrates was characterized. The shear strength test was carried out using the tensile tester to verify the fused sample material joint strength. The measured joint strength was 50 MPa which is stronger than previous attempts and the directly bonded sample as well. This welding technique, using the fixture, overcomes the limitation of allowing for only a small welding region. The sealed area surrounded by welding seams was 418 mm^2, which is much wider compared to the results of previous attempts in the literature. Moreover, the simple microfluidic channel assembly was fabricated using femtosecond laser machining and welding techniques to verify the feasibility of this production method. The experiment clearly demonstrated that glass welding and machining techniques using commercial femtosecond laser systems can increase the potential for sealing applications in microfluidic devices and precision manufacturing.

Chapter 5: Fabrication of Long Period Grating in fiber

5.1 Introduction

Long period fiber grating (LPFG) has been studied as a platform for environment sensors for refractive index (RI) [71], temperature [72], strain [73], liquid level [74], humidity [75], and pressure [76]. LPFG couples the light from a guided core mode to forward propagating cladding modes that show attenuation bands at specific wavelengths. LPFG is fabricated by modulating the RI of a fiber core with a certain periodicity in the order of 100 micrometers to a millimeter [77]. Various methods to fabricate LPFGs have been reported during the last two decades, such as ultraviolet (UV) exposure [78], ion implantation [79], CO2 laser irradiation [80], electric arc [81], and mechanically induced fiber deformation [82]. UV laser exposure is the most common process used to fabricate LPFGs in photosensitive optical fibers, such as boron and germanium doped fibers. However, UV-exposed gratings have an unstable reflective index that decays over time, which results in spectral changes and peak loss of the attenuation bands [83]. Compared with those produced through UV-exposure, the LPFGs fabricated by CO2 lasers have high stability regardless of the photosensitivity of their optical fibers. However, they suffer insertion loss because of an unintended physical deformation caused by laser heating [77].

Among LPFG fabrication methods, processes that use femtosecond lasers have attracted attention because of their high flexibility and stability [84]. Localized femtosecond laser pulses lead to permanent changes of RI in a fiber core, even for photo-

insensitive optical fibers. Moreover, LPFGs fabricated by femtosecond lasers have high resistance to thermal decay and greater durability over time [23].

In conventional LPFG fabrication, each grating is individually inscribed at the fiber-core by multiple scans of the laser beam. The laser beam is irradiated only onto a single side of the fiber, which results in asymmetric core index modification. Because asymmetric index modification causes large polarization dependent loss [85], several processes have been reported that achieve symmetric index modification, such as twisted grating inscription [86], symmetric laser irradiation [87], and pre-processes at cladding [88]. However, those studies are limited to CO2 laser fabrication, so that symmetric index modification is still challenging for femtosecond-laser-based LPFG fabrication.

In this study, I propose a new strategy for femtosecond laser based LPFGs fabrication. In the proposed process, the laser beam is irradiated in the fiber-core while the fiber is moved along the fiber-axis as in the conventional process. A difference compared to the conventional process, here, is that the fiber rotates in a radial direction during the laser scanning along the fiber-axis. As a result, the index modulation with a screw shape is formed in the fiber-core by a single-path scanning process. The fabricated LPFG with a screw shape was compared to the LPFGs fabricated by conventional scanning method with respect to the manufacturing time, reproducibility, and sensing capability. The screw-shaped LPFG was evaluated for RI sensing applications using various concentrations of glycerin solution.

5.2 Sensing principle of LPFG

Structures of periodically modified refractive index change in fiber cores couple light from a guided core mode to forward propagating cladding modes that show attenuation bands at specific wavelengths in the transmission spectrum [19]. The periodic-matching of a long-period fiber (LPFG) results in wavelengths of the refractive index change between fundamental core mode and propagating cladding modes. Moreover, it demonstrates the sensing ranges of the LPFG induced by femtosecond laser. The phase-matching between the forward travelling fundamental core and exterior cladding is found to operate with wavelength

$$\lambda = (\delta n_{eff})\Lambda \tag{5.1}$$

where Λ is the grating periodicity of the LPFG and δn_{eff} is the difference of the corresponding refraction index between the fundamental core and cladding mode, which is satisfied by [89]

$$\delta n_{eff} = n_{core} - n_{cl} \tag{5.2}$$

In this equation, n_{core} and n_{cl} are the refractive indexes of the core and cladding modes, respectively. The principle of refractive index sensing is explained by the mechanism of coupling wavelengths between fundamental core mode and propagating cladding mode known as phase-matching condition. The effective indexes are dependent on the indexes and radii of the core and cladding. The core is represented by n_1, n_2, and n_3, while the cladding and surrounding indexes are represented by $n_2 < n_{eff} < n_l$ and $n_3 < n_{cl} < n_2$.

These equations explain that the resonant wavelength of the coupling is a function which affects the indexes of cladding modes and the grating period. The indexes and radii the of core and cladding are the main variables for the effective indexes, and the effective indexes of the cladding modes are crucial for the surrounding RI (n_3). A difference of surrounding index shifts the effective index of cladding modes **(n_{cl})** with the higher-order modes. The coupling wavelength which relies on n_{cl} coincides with a precise cladding mode. As a consequence, modification of the ambient index (n_3) will change the value of λ. The ambient index (n_3) seems less than the effective index of cladding mode (n_{cl}) with curbing the RI measurements. Ambient index modulation does not influence the fundamental mode guided into fiber core for a typical single mode fiber. The grating period stays constant in steady state external temperature and strains. Hence, under the effect of ambient index, $n_3(d\Lambda/dn_3)$, shifting vibrancy cladding mode is given by [90]

$$\frac{d\lambda}{dn_3} = \frac{d\lambda}{dn_{cl}} \frac{dn_{cl}}{dn_3} \tag{5.3}$$

A negative directional shift in the coupling wavelength, $(d\lambda/dn_{cl}) < 0$, results in the effective index which rises in the cladding mode for the operational band in normal region. Thus, an RI response of LPFG is typically shown as a negative spectral shift of transmission in contact with any RI higher than air.

5.3 Experimental setup and Fabrication

Femtosecond laser systems were prepared to demonstrate LPFG fabrication with two different methods as shown in Figure 5.1. A femtosecond laser (Spectra-Physic ultrafast Ti:Sapphire laser) used in this system has a 120 fs pulse width and 1 kHz repetition rate at a central wavelength of 800 nm. The laser beam was guided into a microscope and focused into the fiber core by using a 50X objective lens with numerical aperture of 0.55. An electronic shutter with a computer assisted control system was used to timely irradiate the laser beam at the desired focal position. Index modification was observed during laser irradiation by a CCD camera installed above the dichroic mirror. Single-mode optical fiber (Fiber Instrument Sales) was placed on a 4-axis stage for automatic positioning. Two ends of the fiber were individually connected to a spectrum analyzer (PHOTONETICS Walics) and a broad band light source (AFC BBS-1550) for monitoring changes in transmission spectrum.

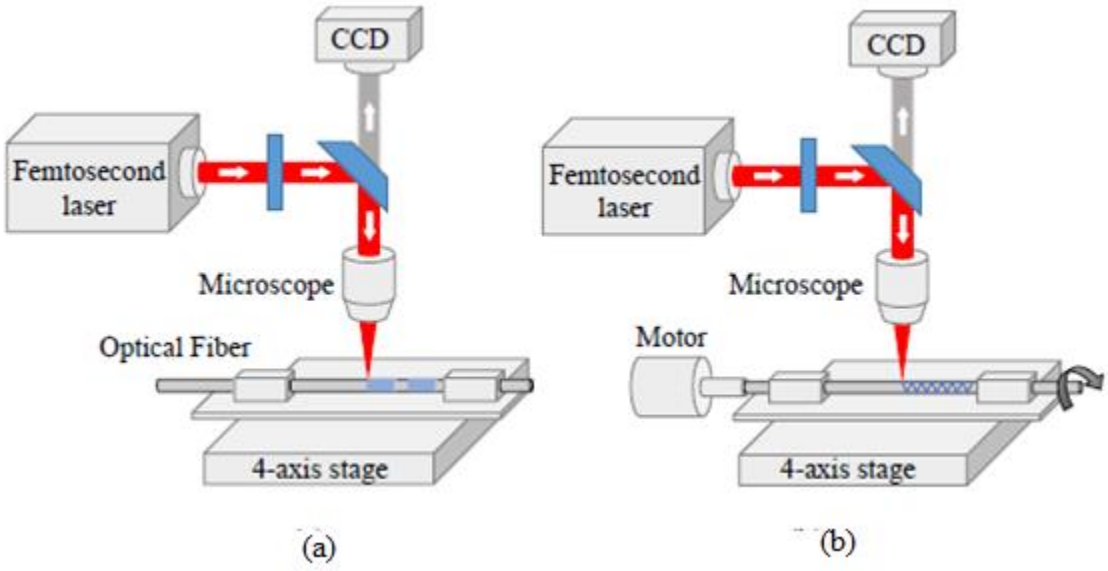

Figure 5.1 Schematics of the femtosecond laser system for LPFG fabrication by (a) multi-path scanning and (b) single-path scanning.

Figure 5.1 (a) shows a schematic diagram of the conventional LPFG fabrication that uses the multi-path scanning method. Therein, discrete gratings are formed along the fiber axis and each grating is inscribed with a zig-zag pattern. Figure 5.1 (b) shows a schematic diagram of laser inscription with a single scanning method for fabrication of the LPFG with a screw-shaped grating. The laser inscribes the fiber core along the transverse direction while the fiber rotates. A DC motor was additionally used to rotate the fiber. Because the RI modification is continuously formed while the fiber moves along the fiber axis, this method is termed single-path scanning.

5.4 Fabrication result and discussion

5.4.1 Conventional LPFG

Conventional LPFGs were fabricated at pure silica core single mode fiber through the femtosecond laser fabrication with multi-path scanning. Each grating was formed by inscribing zig-zag patterns line by line as shown in Figure 5.2 (a). The zig-zag pattern was formed with a line-by-line inscription of 100-μm-length lines with an interval of 1 μm. Figure 5.2 (b) shows the fabrication result at the region of core index modification, as produced the multi-path scanning method. The femtosecond laser power was 1.53 μW and the travel speed along the fiber axis was 30 μm/s. The index change area had a length of 100 μm. Inside the fiber core, no damage or cracks were observed in either core or cladding. Therefore, background loss can be ignored in the transmission results.

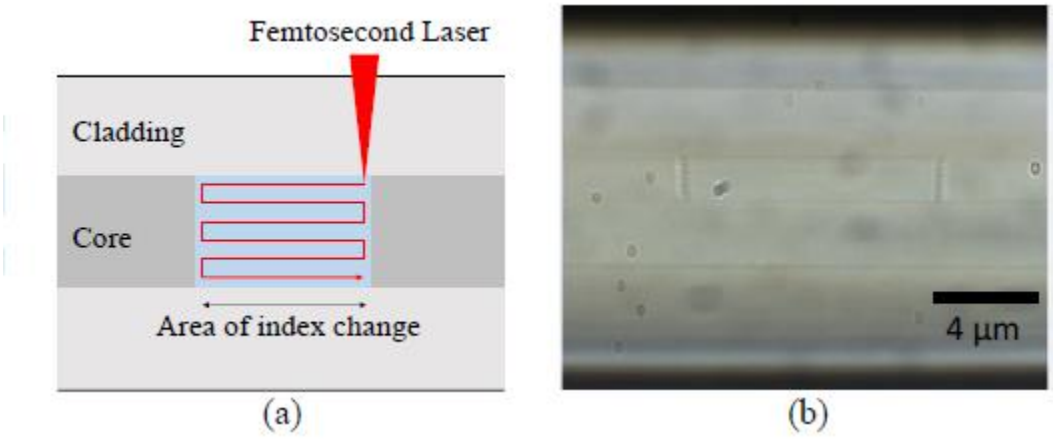

Figure 5.2 Schematics of the femtosecond laser system for LPFG fabrication by (a) multi-path scanning and (b) single-path scanning.

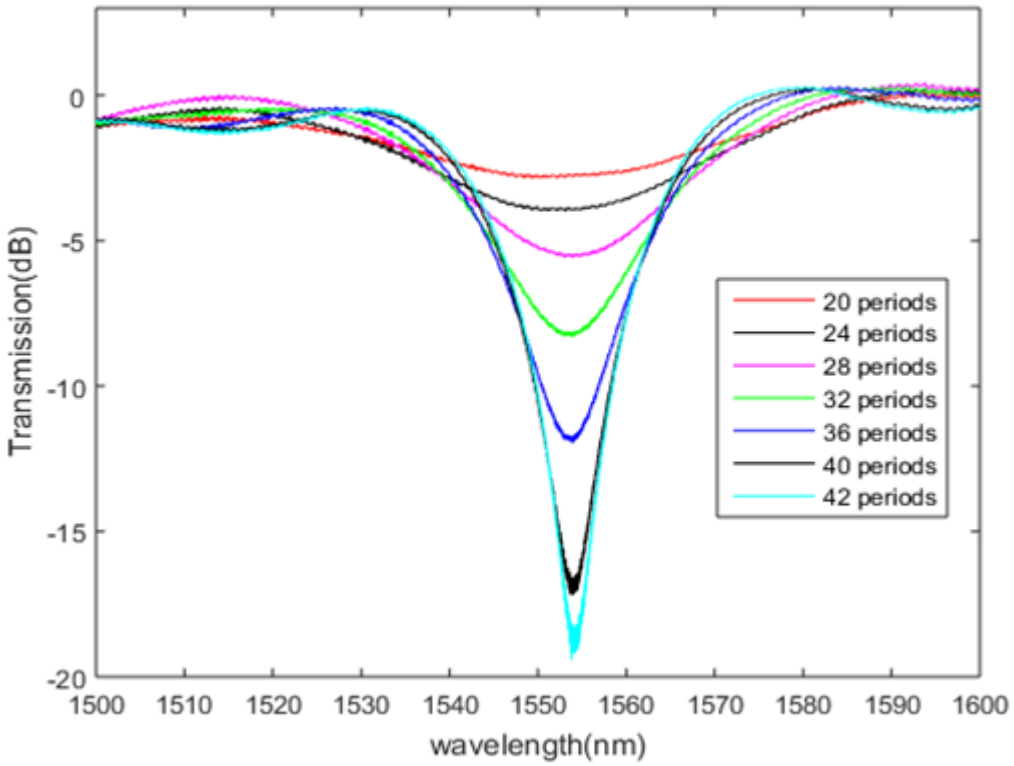

Figure 5.3 Transmission dips of the LPFGs with different numbers of periods. Transmission dip decreases after 42 periods.

Figure 5.3 shows the spectral growth of LPFGs transmission dip for different numbers of periods: namely, 20, 24, 28, 32, 36, 40, and 42. The transmission dip occurs from the LPFGs with 20th periods. A larger number of periods causes deeper transmission dip. The transmission spectrum was measured until loss peak of the LPFG reached maximum value. The transmission dip of the LPFGs with 42 periods reaches approximately 19.5 dB at 1553 nm and it has full width at half maximum (FWHM) of 8 nm. The LPFG with 42 periods have a total length of 17.77 mm.

The RI dependence of the loss peak wavelength was investigated for the three LPFGs with 42 periods. The fabricated LPFGs were immersed in different concentrations of glycerin solutions ranging from 0% to 80%. RIs of the glycerin solution at room temperature were 1.3330, 1.3448, 1.3575, 1.3707, 1.3841, 1.3981, 1.4130, 1.4279, and 1.4429 for concentrations of 0, 10, 20, 30, 40, 50, 60, 70, and 80%, respectively.

Figure 5.4 shows the spectral shifts of the LPFGs fabricated with 42 periods. As the glycerin concentration increases, a blue shift of the loss peaks is observed. Figure 5.5 shows the RI characterization for the LPFGs with different periods fabricated by multi-path scanning. The RI sensitivity of the conventional LPFGs was approximately 36 ~ 39 nm/RIU in the range of 0% to 70% glycerin concentration. Moreover, the peak shift dramatically increased in the range of 70% to 80% glycerin concentration.

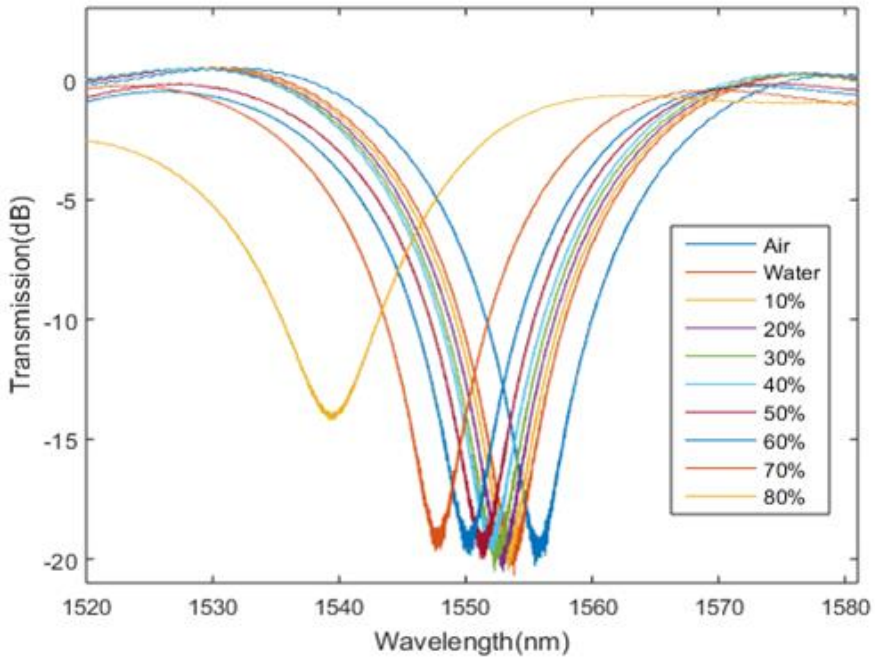

Figure 5.4 Spectral growths of the transmission dips for the LPFGs fabricated by multi-path scanning with 42 periods. The transmission dip decreased at 80% glycerin concentration.

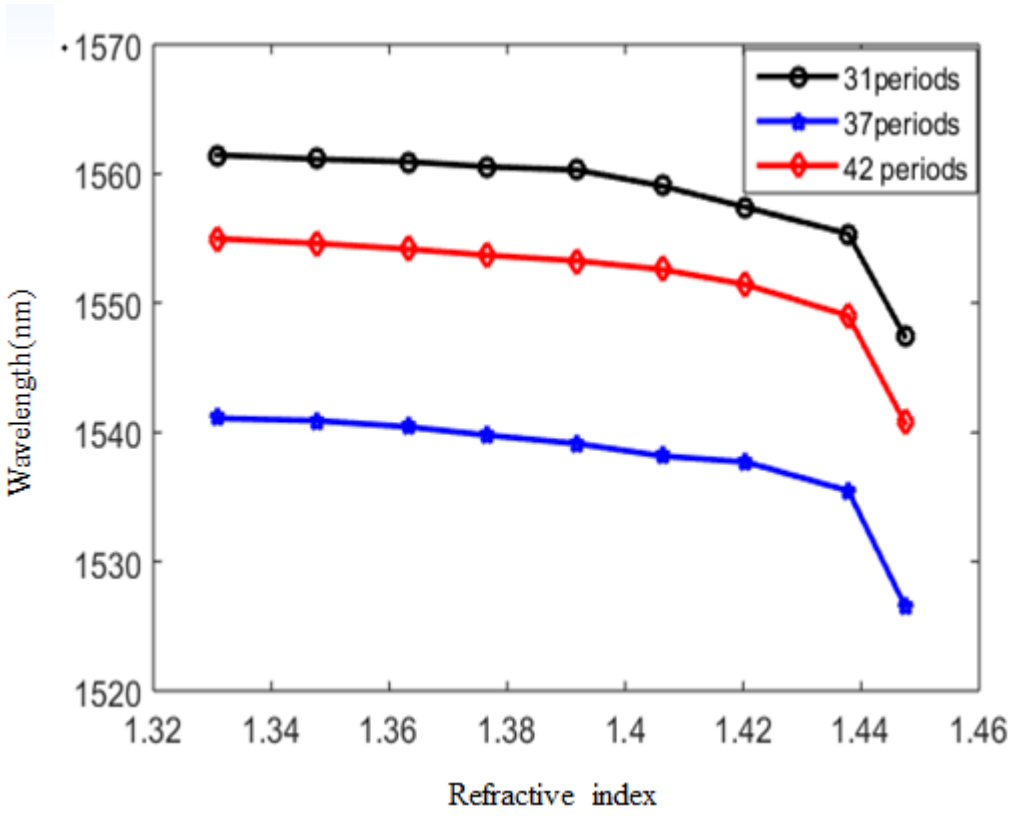

Figure 5.5 Refractive index characterization of the LPFGs fabricated by multipath scanning.

5.4.2 Screw-shape LPFG

LPFGs with screw shapes were fabricated at pure silica core single mode fiber through the technique of single-path scanning by the femtosecond laser, as shown in Figure 5.6 (a). In order to form a screw shape in the grating, laser inscription along the fiber axis and rotation of the fiber were performed simultaneously. During the laser inscription, the fiber was continuously rotated at 45 rpm using a DC motor. In order to rotate the fiber at constant speed while minimizing run-out, the fiber was pulled from both ends to maintain

tension during laser irradiation. The measured fiber run-out was less than 1 μm. Figure 5.6 (b) shows the fabrication result of the 100 μm-length grating with the screw shape by the multi-path scanning method. The femtosecond laser power was 1.53 μW and the travel speed along the fiber axis was 10 μm/s.

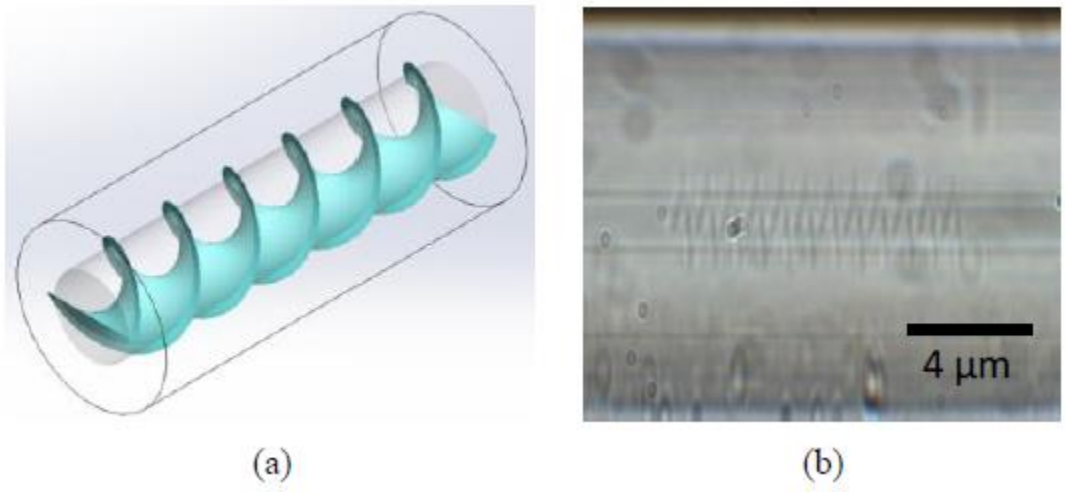

Figure 5.6 (a) Schematic of the screw-shaped LPFGs fabricated by the single-path scanning and (b) the fabrication result of the LPFG with a screw shape by a single-path scanning.

Figure 5.7 shows the spectral growth of the transmission dips for the screw-shaped LPFGs with a variable number of periods: namely, 80, 90, 97, and 100. The periodicity of gratings was 450 μm. Although the screw-shaped LPFGs were fabricated with a different number of periods, their spectral deviation was only 0.22 nm. For the screw-shaped LPFGs with 100 periods, the transmission dip reached 21 dB at 1548 nm and the FWHM was 3.5 nm. The total length of LPFG was 44.65 mm and the fabrication time was 17 min in duration which is relatively short time compared to conventional LPF fabrication time (50 min). The fabrication time was reduced because the laser scanning was performed in

a single path. In addition, the screw-shaped LPFGs generated deeper and narrower dips when compared with the conventional LPFGs, because of azimuthally symmetric index change in the gratings.

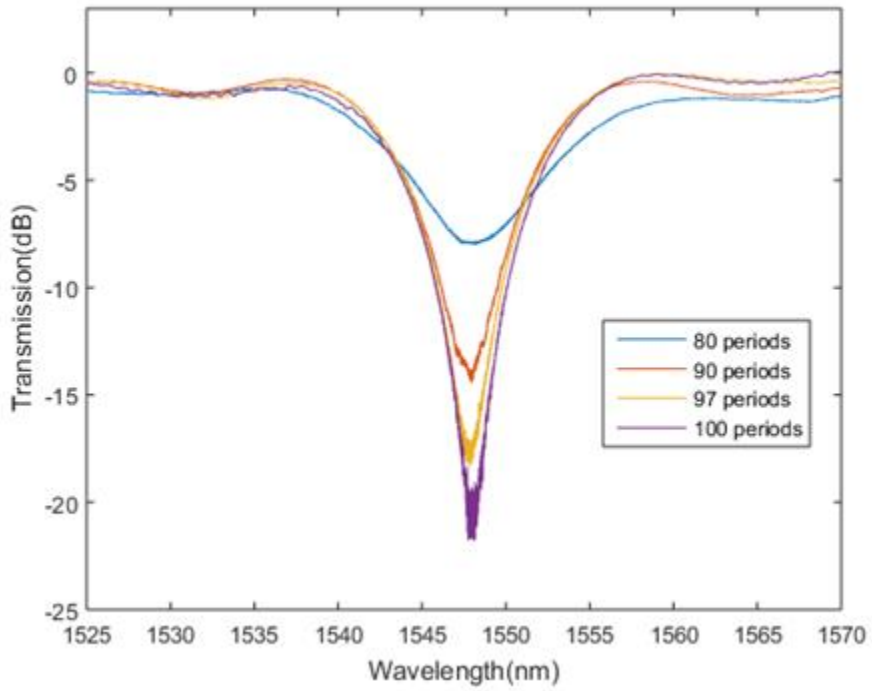

Figure 5.7 Transmission dips of the screw-shaped LPFGs with different number of gratings.

Figure 5.8 shows the transmission spectra of the screw-shaped LPFGs with 100 periods, when immersed in glycerin solution with variable concentrations. Their total length was 44.65 mm, respectively. Similar to the conventional LPFGs, the blue shift occurs in transmission dips as the surrounding RI increases. A deeper dip was observed for the 44.65-mm-long LPFGs in 80% of glycerin solution than for the 22.54-mm-long LPFGs. Figure 5.9 shows the RI sensitivity of the screw-shaped LPFGs with different numbers of periods. Both LPFGs had similar RI sensitivity regardless of the total grating length,

period, or laser power. The RI sensitivity was approximately 48 ~ 51 nm/RIU in the range of 0% to 70% glycerin concentration. The peak shift dramatically increases in the range of 70% to 80% glycerin concentration. By comparing it to the conventional LPFGs, the sensitivity of the screw-shaped LPFGs is better.

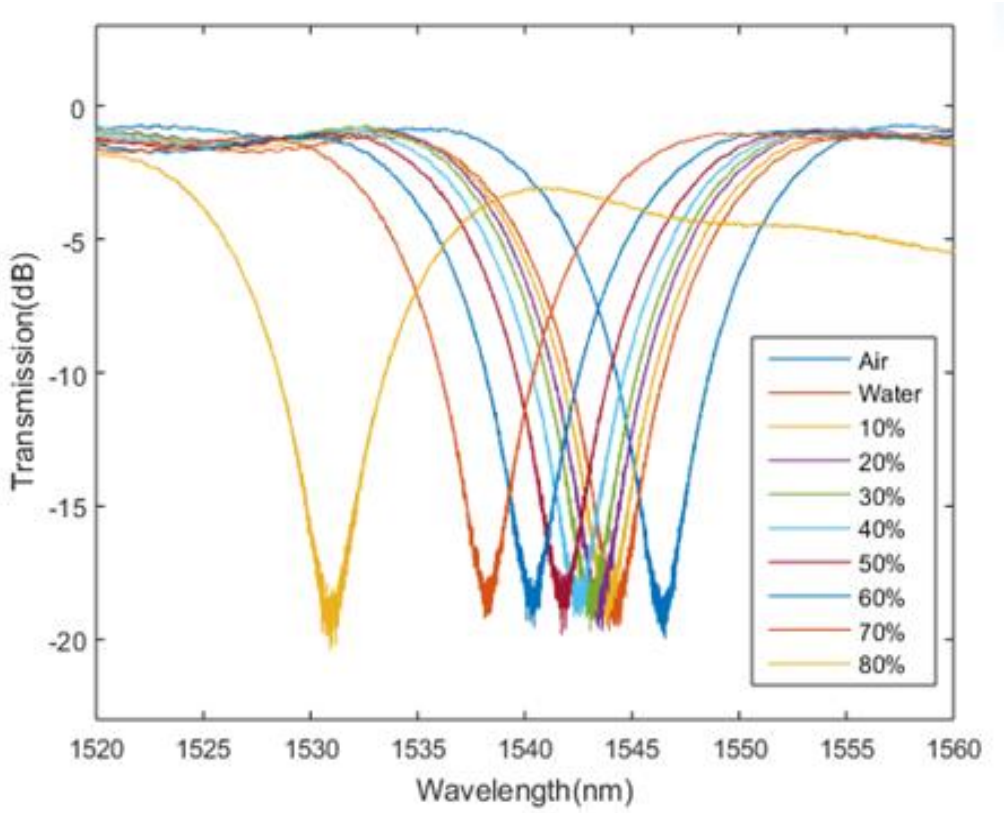

Figure 5.8 Spectral shift of the LPFG with 100 periods. The transmission dip remains at 80% glycerin concentration.

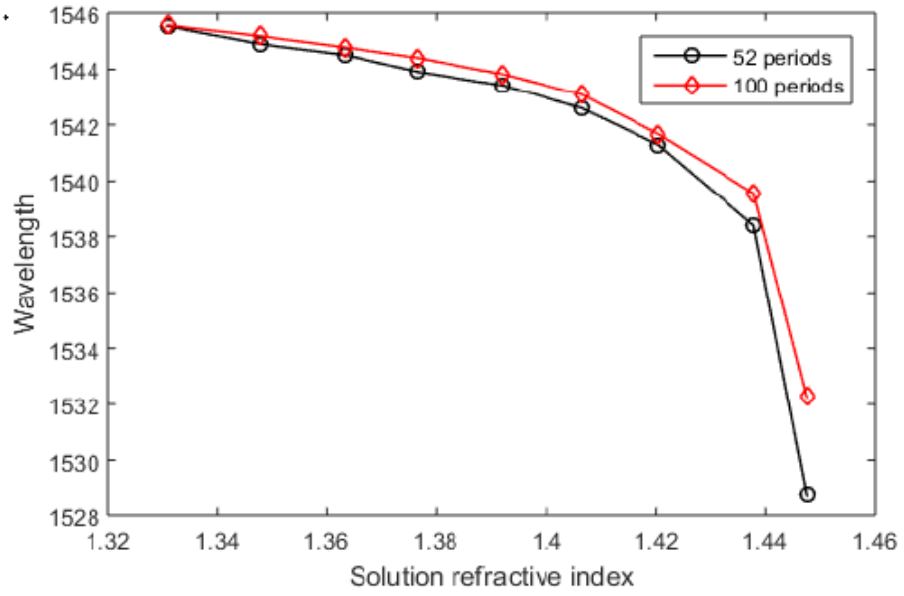

Figure 5.9 Refractive index characterization of the screw-shaped LPFGs fabricated by single-path scanning. The sensitivity of screw-shaped LPG is better than conventional LPG (from 36~39 nm/RIU to 48~51 nm/RIU)

5.4.3 The screw-shaped LPFG with complicated pitches

LPFG is vulnerable to fiber bending and transmission dip normally decreases as fiber bending curvature increases. Several sensors for measuring bending curvature, vibration, and acoustic wave have been reported in relation to this LPFG's behavior [91-96]. However, attenuation dip will disappear as bending curvature increases. Therefore, LPFG is unable to sense any target substrates or properties such as surrounding refractive index, vibration and temperature. In order to solve those issues, LPFG fabricated by rotating fibers can provide a viable alternative. Reverse bending effect is investigated in helical LPFG by writing complex index modulations. As shown in Figure 9, the pitch of the screw shape of the index modification can be controlled by adjusting the feed rate along the fiber axis. As the feed rate increases in speed, the pitch of the screw becomes longer.

Based on this process, a new structure of the LPFG with a screw shape is proposed here, as shown in Figure 5.10,: a screw-shaped LPFG with complex index modulation. This structure is generated by adjusting the feed rate repeatedly. Each coloured lines in Figure 5.10 represents the switching position of the feed rate. As the feed rate was switched at each line, the pitch of the screw-shaped index modification was mixed along the fiber axis.

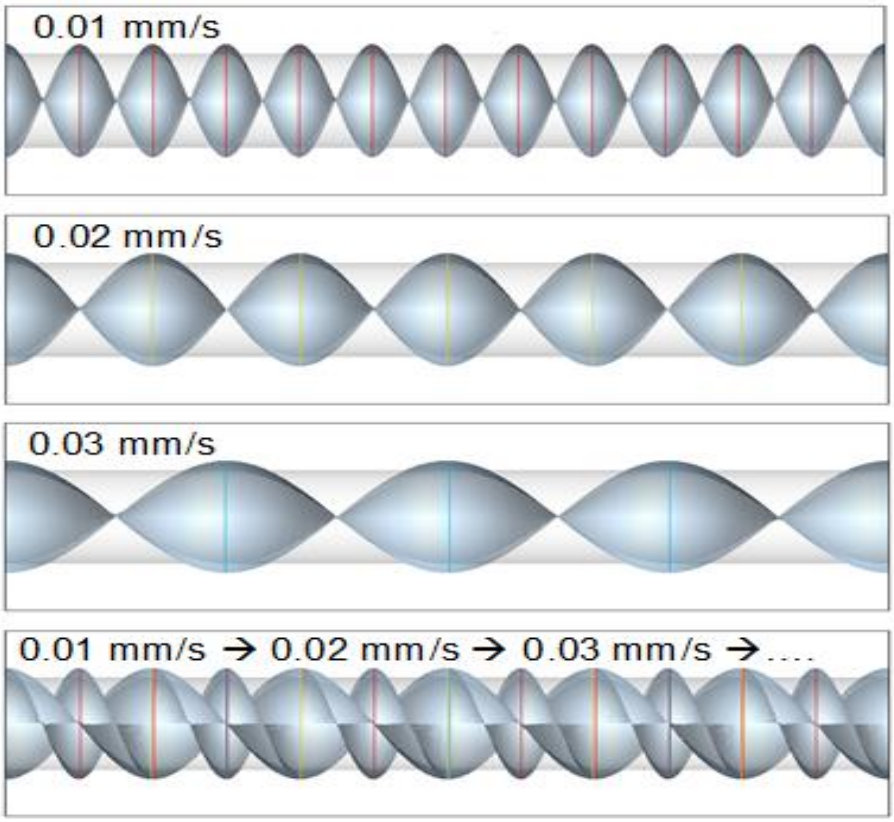

Figure 5.10 Diagrams of the LPFG with screw-shape of different pitch. Three different helical refractive index changes were integrated by overlapping laser scans and complex screw-shaped LPG was fabricated.

A screw-shaped LPFG with complex pitches was fabricated and its bending effect was evaluated. Fiber index modifications were produced with five different feed rates: namely,

of 0.01 mm/s, 0.03 mm/s, 0.05 mm/s, 0.07 mm/s, and 0.09 mm/s along the fiber axis. The screw-shaped LPG with complex pitches was fabricated at each grating with a length of 440 μm. The number of gratings was 60 and its total length was 26.06 mm. Bending effect of the screw-shaped LPG with complex pitches was investigated by applying various weights to the fiber. Figure 5.11 shows transmission dips for the complex helical LPFGs while various weights of 0 N to 17.2×10^{-4} N hanging from the complex helical LPFG. The transmission dip was 13 dB at 1539 nm for the complex helical LPFG when no weight was hanging from it. The transmission dip was increased to 19 dB while the weight of 17.2×10^{-4} N was hanging from it. The transmission dip became deeper as the bending curvature increased. This phenomenon is completely different from what is observed in conventional LPG's spectral variation that transmission dip decreases or disappears as bending curvature increases.

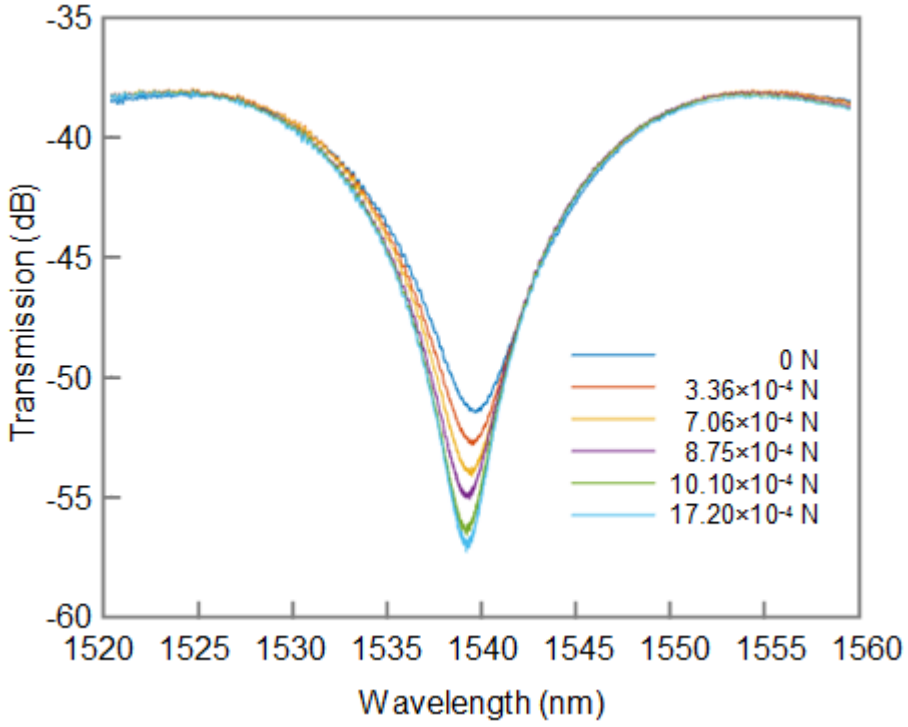

Figure 5.11 Bending characterization of the screw-shaped LPFG with different pitches

5.5 Conclusion

LPFGs with a screw shape were produced by femtosecond laser induced index change, using a single-path scanning technique. Transmission characteristics of the screw-shaped LPFGs and the conventional LPFGs were compared in order to verify the relative reliability of the screw-shaped LPFGs. The fabricated LPFGs with a screw shape had no significant insertion loss, as did the conventional LPFGs. Moreover, compared to the conventional LPFGs, deeper and narrower transmission dips were observed in the screw-shaped LPFGs. The experiment showed relatively large transmission dips up to 21 dB with FWHM of 3.5 nm. The RI sensitivity of the screw-shaped LPFGs was approximately 48 ~ 51 nm/RIU. The screw-shaped LPFG has improved performance

because its index change was inscribed azimuthally at the fiber core by the proposed single-path method. In addition, the screw-shaped LPFGs with complex pitches were produced by adjusting the feed rate of the fiber along the fiber axis. Reverse bending effect was observed for the screw-shaped LPFG with complex pitches. Unlike the conventional LPFGs, the transmission dip of the proposed LPFG sensor was measured although the curvature increases. Accordingly, this type of LPFG can be used as a micro unit scale or bending sensor. Moreover, the screw-shaped LPFGs with complex pitches can be an alternative to the LPFG sensors used for monitoring structural parameters under harsh environmental conditions that produce significant bending or severe vibration.

Chapter 6 Conclusion and future work

6.1 Conclusion

Three types of manufacturing techniques (GRIN lens, laser welding and long period grating sensor) using femtosecond laser pulse filamentation were presented in this thesis. Filament propagation in transparent materials was investigated as a first step, because the controllable filaments can modify the refractive index or the structure of glass materials. Pulse energy varies the area and length of filament propagation, and the filament voids with/without damage were compared to verify the effect of transmit light intensity and noise using the spectrum analyzer. The concept of gradient index lens was introduced, which uses 3-D photonic structures inscribed by ultrashort pulse filaments. This process gradually increases refractive index of glass materials, modified by controlled scanning speed and variable pulse overlapping. As a result, laser light became focused with a high intensity. I believe that in the future this technique can replace existing methods. Advantages of GRIN lens fabrication include simple processing and affordable costs for manufacturers.

A second fabrication technique using femtosecond laser in transparent material, welding of two glass slides was demonstrated using a customized fixture. A wider sealing area than those made possible by the previous work was achieved. This required securing a wide optical contact area to the fixture. Experiments conducted produced sealed areas surrounded by welding seams that reached a size of 418 mm^2. To demonstrate a more

specific application, a simple microfluidic channel assembly was fabricated using femtosecond laser machining and welding techniques. The liquid smoothly flowed into the micro-channel without leakage due to the welding seams maintaining their integrity around the channel. Finally, an LPFG with a helical-shaped refractive index change was investigated. A deeper and narrower transmission dip was achieved due to the azimuthally modified refractive index of the optical fiber. Its shape had a secondary advantage, in that fabrication time was also improved when compared to the conventional LPG fabrication method. Unlike the conventional LPG, the screw-shaped LPG with complex pitches showed greater transmission dip as the curvature of the sensor increased. This new type of LPG sensor can operate as a micro-unit scale or a bending sensor that does not lose its functionality under harsh environments such as significant bending or severe vibration.

6.2 Future work

Before the concept of GRIN lens fabrication method will be taken up by industry, the precise measurement of refractive index change and the size of pulse filaments according to laser parameters (power, and index change by pulse overlapping rates) must be investigated in greater depth. Researchers must determine and control the working distance of the GRIN lens. Although a 3-axis stage was effectively used in this study to prove the feasibility of GRIN lenses, productivity of GRIN lens can be improved. Areas for future advancements include fabrication time and lens diameter. These advancements

will require that researchers precisely measure refractive indexes and the size of filaments. Figure 6.1 shows how GRIN lens fabrication may be improved with shorter fabrication time and lager diameter. Due to a combination of rotating stage with 3-axis stage, a single-scanning path technique can produce uniform refractive index change. The number of laser writing layers will always be determined by the lens diameter, but fabrication time will definitely be reduced with the proposed method.

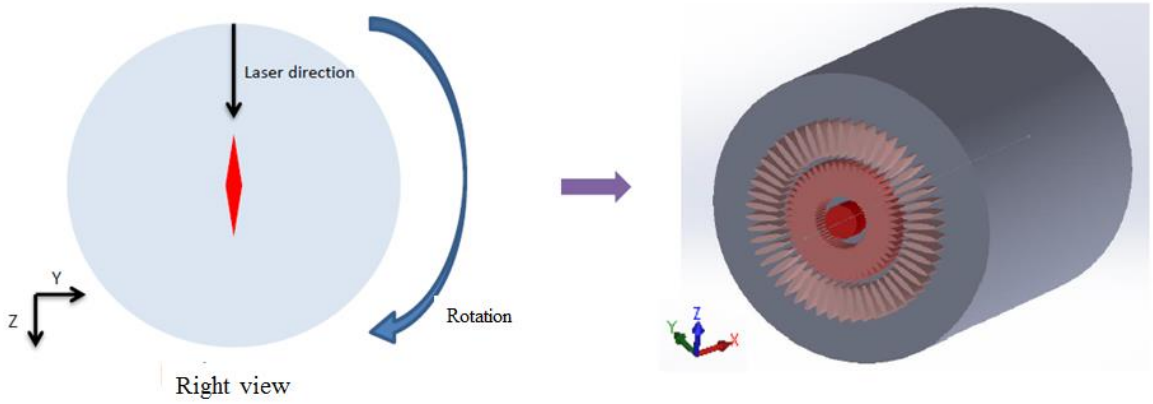

Figure 6.1 GRIN lens fabrication method using rotational stage.

In a glass welding study using femtosecond lasers, two glass slides were shown to bend slightly due to the force applied by the fixture. In the experimental fabrication processes conducted as part of this research project, more than 3 hours elapsed before target areas were properly fused and sealed, because the area joint strength must be larger than the bending force for optical contact induced by the customized fixture. I believe that future

studies on joint strength, pulse energy, and welding seams will help to improve the required fabrication time for producing microfluidic devices with laser welding.

Optical fiber sensors are required for reliability and productivity (fabrication time and cost effective) in manufacturing processes. Although the fabrication time of screw shaped LPFGs was much improved compared to the conventional LPG, it can be further improved if the use of femtosecond laser with higher repetition rate (> 1 kHz) is explored. More precise rotary stage, without significant vibration or run-out, needs to be developed in the interest of sensing reliability. Improved rotary stage may produce better symmetric refractive index change resulting in fabrication flexibility and improved performance. Moreover, the bending effect of screw-shaped LPFG sensors first developed in this thesis has not been analyzed in terms of physics (why reverse spectral shift appears compared to the conventional LPFG). This is only phenomenon of light behavior in the optical fiber with a complex structure of refractive index. In order to use such a bending effect as a multipurpose sensor, physical analysis of light behavior induced by complex pitches are required and more experimental results based on physical analysis need to be investigated.

Bibliography

1. Maiman, T.H., *Stimulated Optical Radiation in Ruby.* Nature, 1960. **187**(4736): p. 493-494.
2. Fork, R.L., B.I. Greene, and C.V. Shank, *Generation of Optical Pulses Shorter Than 0.1 Psec by Colliding Pulse Mode-Locking.* Applied Physics Letters, 1981. **38**(9): p. 671-672.
3. Strickland, D. and G. Mourou, *Compression of Amplified Chirped Optical Pulses.* Optics Communications, 1985. **56**(3): p. 219-221.
4. Jaeggi, B., et al., *Influence of the Pulse Duration in the ps-Regime on the Ablation Efficiency of Metals*, in *Lasers in Manufacturing 2011: Proceedings of the Sixth International Wlt Conference on Lasers in Manufacturing, Vol 12, Pt B*, M. Schmidt, et al., Editors. 2011. p. 164-171.
5. Schaffer, C.B., J.F. Garcia, and E. Mazur, *Bulk heating of transparent materials using a high-repetition-rate femtosecond laser.* Applied Physics a-Materials Science & Processing, 2003. **76**(3): p. 351-354.
6. Veiko, V.P., *Laser-assisted microshaping*, in *Laser-Assisted Microtechnology 2000*, V.P. Veiko, Editor. 2001, Spie-Int Soc Optical Engineering: Bellingham. p. 93-104.
7. Mao, S.S., et al., *Dynamics of femtosecond laser interactions with dielectrics.* Applied Physics a-Materials Science & Processing, 2004. **79**(7): p. 1695-1709.
8. Hamad, A., *Effects of Different Laser Pulse Regimes (Nanosecond, Picosecond and Femtosecond) on the Ablation of Materials for Production of Nanoparticles in Liquid Solution*. 2016. p. 21.
9. Le Harzic, R., et al., *Comparison of heat-affected zones due to nanosecond and femtosecond laser pulses using transmission electronic microscopy.* Applied Physics Letters, 2002. **80**(21): p. 3886-3888.
10. Del Fatti, N., A. Arbouet, and F. Vallee, *Femtosecond optical investigation of electron-lattice interactions in an ensemble and a single metal nanoparticle.* Applied Physics B-Lasers and Optics, 2006. **84**(1-2): p. 175-181.
11. Rousse, A., et al., *EFFICIENT K-ALPHA-X-RAY SOURCE FROM FEMTOSECOND LASER-PRODUCED PLASMAS.* Physical Review E, 1994. **50**(3): p. 2200-2207.
12. Yan, X. and Y. Ohishi, *Supercontinuum generation in a tapered tellurite microstructured optical fiber*, in *International Symposium on Photonics and Optoelectronics 2014*, Z. Zhou, Editor. 2014.
13. Davis, K.M., et al., *Writing waveguides in glass with a femtosecond laser.* Optics Letters, 1996. **21**(21): p. 1729-1731.
14. Glezer, E.N., et al., *Three-dimensional optical storage inside transparent materials (vol 21, pg 2023, 1996).* Optics Letters, 1997. **22**(6): p. 422-422.

15. Birngruber, R., et al., *FEMTOSECOND LASER TISSUE INTERACTIONS - RETINAL INJURY STUDIES.* Ieee Journal of Quantum Electronics, 1987. **23**(10): p. 1836-1844.
16. Cerullo, G., et al., *Femtosecond micromachining of symmetric waveguides at 1.5 mu m by astigmatic beam focusing.* Optics Letters, 2002. **27**(21): p. 1938-1940.
17. Sudrie, L., et al., *Writing of permanent birefringent microlayers in bulk fused silica with femtosecond laser pulses.* Optics Communications, 1999. **171**(4-6): p. 279-284.
18. Huang, S.M., et al., *Three dimensional optical storage by use of ultrafast laser*, in *Optical Data Storage 2003*, M. Oneill and N. Moyagawa, Editors. 2003. p. 264-268.
19. Vengsarkar, A.M., et al., *Long-period fiber gratings as band-rejection filters.* Journal of Lightwave Technology, 1996. **14**(1): p. 58-65.
20. Tamaki, T., et al., *Welding of transparent materials using femtosecond laser pulses.* Japanese Journal of Applied Physics Part 2-Letters & Express Letters, 2005. **44**(20-23): p. L687-L689.
21. Choi, J., et al., *Femtosecond laser written embedded diffractive optical elements and their applications*, in *Frontiers in Ultrafast Optics: Biomedical, Scientific, and Industrial Applications X*, A. Heisterkamp, et al., Editors. 2010.
22. Streltsov, A.M. and N.F. Borrelli, *Fabrication and analysis of a directional coupler written in glass by nanojoule femtosecond laser pulses.* Optics Letters, 2001. **26**(1): p. 42-43.
23. Kondo, Y., et al., *Fabrication of long-period fiber gratings by focused irradiation of infrared femtosecond laser pulses.* Optics Letters, 1999. **24**(10): p. 646-648.
24. Yamada, K., et al., *Multilevel phase-type diffractive lenses in silica glass induced by filamentation of femtosecond laser pulses.* Optics Letters, 2004. **29**(16): p. 1846-1848.
25. Huang, H., L.M. Yang, and J. Liu, *Direct welding of fused silica with femtosecond fiber laser*, in *Laser-Based Micro- and Nanopackaging and Assembly Vi*, F.G. Bachmann, et al., Editors. 2012.
26. Kasaai, M.R., et al., *The interaction of femtosecond and nanosecond laser pulses with the surface of glass.* Journal of Non-Crystalline Solids, 2003. **319**(1-2): p. 129-135.
27. Zhang, J., et al., *157-nm laser-induced modification of fused-silica glasses*, in *Laser Applications in Microelectronic and Optoelectronic Manufacturing Vi*, M.C. Gower, et al., Editors. 2001. p. 125-132.
28. Schaffer, C.B., et al., *Micromachining bulk glass by use of femtosecond laser pulses with nanojoule energy.* Optics Letters, 2001. **26**(2): p. 93-95.
29. Gattass, R.R., L.R. Cerami, and E. Mazur, *Micromachining of bulk glass with bursts of femtosecond laser pulses at variable repetition rates.* Optics Express, 2006. **14**(12): p. 5279-5284.

30. Horn, A., E.W. Kreutz, and R. Poprawe, *Ultrafast time-resolved photography of femtosecond laser induced modifications in BK7 glass and fused silica.* Applied Physics a-Materials Science & Processing, 2004. **79**(4-6): p. 923-925.
31. Eisenberg, H.S. and Y. Silberberg, *Phase defects in self-focusing of ultrashort pulses.* Physical Review Letters, 1999. **83**(3): p. 540-543.
32. Marburger, J.H., *Self-focusing: Theory (Reprinted from vol 4, pg 35-110, 1975)*, in *Self-Focusing: Past and Present: Fundamentals and Prospects*, R.W. Boyd, S.G. Lukishova, and Y.R. Shen, Editors. 2009. p. 25-+.
33. Schaffer, C.B., A. Brodeur, and E. Mazur, *Laser-induced breakdown and damage in bulk transparent materials induced by tightly focused femtosecond laser pulses.* Measurement Science and Technology, 2001. **12**(11): p. 1784-1794.
34. Sheehy, B., et al., *Single and multiple electron dynamics in the strong field limit*, in *Multiphoton Processes 1996*, P. Lambropoulos and H. Walther, Editors. 1997. p. 106-117.
35. Yu, P.Y. and M. Cardona, *Fundamentals of Semiconductors: Physics and Materials Properties, Fourth Edition*, in *Fundamentals of Semiconductors: Physics and Materials Properties, Fourth Edition*. 2010. p. 1-775.
36. Yablonovitch, E. and N. Bloembergen, *AVALANCHE IONIZATION AND LIMITING DIAMETER OF FILAMENTS INDUCED BY LIGHT-PULSES IN TRANSPARENT MEDIA.* Physical Review Letters, 1972. **29**(4): p. 907-+.
37. Chin, S.L., *Filamentation Nonlinear Optics*, in *Lectures on Ultrafast Intense Laser Science 1*, K. Yamanouchi, Editor. 2011. p. 241-275.
38. Couairon, A., *Filamentation length of powerful laser pulses.* Applied Physics B-Lasers and Optics, 2003. **76**(7): p. 789-792.
39. Chan, J.W., et al., *Structural changes in fused silica after exposure to focused femtosecond laser pulses.* Optics Letters, 2001. **26**(21): p. 1726-1728.
40. Glezer, E.N., et al., *Three-dimensional optical storage inside transparent materials.* Optics Letters, 1996. **21**(24): p. 2023-2025.
41. Fertein, E., et al., *Refractive-index changes of standard telecommunication fiber through exposure to femtosecond laser pulses at 810 cm.* Applied Optics, 2001. **40**(21): p. 3506-3508.
42. Homoelle, D., et al., *Infrared photosensitivity in silica glasses exposed to femtosecond laser pulses.* Optics Letters, 1999. **24**(18): p. 1311-1313.
43. Ahmed, F., et al., *Display glass cutting by femtosecond laser induced single shot periodic void array.* Applied Physics a-Materials Science & Processing, 2008. **93**(1): p. 189-192.
44. Wu, Z.X., et al., *Filamentation and temporal reshaping of a femtosecond pulse in fused silica.* Physical Review A, 2003. **68**(6).
45. Braun, A., et al., *SELF-CHANNELING OF HIGH-PEAK-POWER FEMTOSECOND LASER-PULSES IN AIR.* Optics Letters, 1995. **20**(1): p. 73-75.
46. Wu, Z.X., et al., *Multiple foci and a long filament observed with focused femtosecond pulse propagation in fused silica.* Optics Letters, 2002. **27**(6): p. 448-450.

47. Tzortzakis, S., et al., *Self-guided propagation of ultrashort IR laser pulses in fused silica.* Physical Review Letters, 2001. **87**(21).
48. Marcinkevicius, A., et al., *Effect of refractive index-mismatch on laser microfabrication in silica glass.* Applied Physics a-Materials Science & Processing, 2003. **76**(2): p. 257-260.
49. Ahmed, F., et al., *Near-field modification of femtosecond laser beam to enhance single-shot pulse filamentation in glass medium.* Applied Physics a-Materials Science & Processing, 2014. **114**(4): p. 1161-1165.
50. Chin, S.L., et al., *The propagation of powerful femtosecond laser pulses in optical media: physics, applications, and new challenges.* Canadian Journal of Physics, 2005. **83**(9): p. 863-905.
51. Houdewalter, S.N. and D.T. Moore, *GRADIENT-INDEX PROFILE CONTROL BY FIELD-ASSISTED ION-EXCHANGE IN GLASS.* Applied Optics, 1985. **24**(24): p. 4326-4333.
52. Beltrami, D.R., et al., *Fabrication and characterization of a planar gradient-index, plasma-enhanced chemical vapor deposition lens.* Applied Optics, 1997. **36**(28): p. 7143-7149.
53. Reed, W.A., M.F. Yan, and M.J. Schnitzer, *Gradient-index fiber-optic microprobes for minimally invasive in vivo low-coherence interferometry.* Optics Letters, 2002. **27**(20): p. 1794-1796.
54. Ye, C., R.R. McLeod, and Ieee, *GRIN lens and GRIN lens array fabrication with diffusion-driven photopolymer*. 2009 Conference on Lasers and Electro-Optics and Quantum Electronics and Laser Science Conference. 2009. 104-105.
55. Visconti, A.J. and J.L. Bentley, *Fabrication of large-diameter radial gradient-index lenses by ion exchange of Na+ for Li+ in titania silicate glass.* Optical Engineering, 2013. **52**(11).
56. Lacroix, F., D. Helie, and R. Vallee, *Optical Bonding Reinforced by Femtosecond Laser Welding*, in *Optical Manufacturing and Testing Ix*, J.H. Burge, O.W. Fahnle, and R. Williamson, Editors. 2011.
57. Kongsuwan, P., et al., *Characterization of Morphology and Mechanical Properties of Glass Interior Irradiated by Femtosecond Laser.* Journal of Manufacturing Science and Engineering-Transactions of the Asme, 2010. **132**(4).
58. Wei, J., et al., *Glass-to-glass anodic bonding process and electrostatic force.* Thin Solid Films, 2004. **462**: p. 487-491.
59. Haisma, J. and G.A.C.M. Spierings, *Contact bonding, including direct-bonding in a historical and recent context of materials science and technology, physics and chemistry - Historical review in a broader scope and comparative outlook.* Materials Science & Engineering R-Reports, 2002. **37**(1-2): p. 1-60.
60. Haisma, J., et al., *Direct bonding and beyond.* Applied Optics, 2007. **46**(27): p. 6793-6803.
61. Haisma, J., et al., *Surface Preparation and Phenomenological Aspects of Direct Bonding.* Philips Journal of Research, 1995. **49**(1-2): p. 23-46.

62. Kongsuwan, P., G. Satoh, and Y.L. Yao, *Transmission Welding of Glass by Femtosecond Laser: Mechanism and Fracture Strength.* Journal of Manufacturing Science and Engineering-Transactions of the Asme, 2012. **134**(1).
63. Horn, A., et al., *Joining of thin glass with semiconductors by ultra-fast high-repetition laser welding.* Laser-Based Micro- and Nanopackaging and Assembly Ii, 2008. **6880**.
64. Richter, S., et al., *Ultrastable Bonding of glass with femtosecond laser bursts.* Frontiers in Ultrafast Optics: Biomedical, Scientific, and Industrial Applications Xiii, 2013. **8611**.
65. Watanabe, W., et al., *Joining of transparent materials by femtosecond laser pulses.* Commercial and Biomedical Applications of Ultrafast Lasers Vii, 2007. **6460**.
66. Tamaki, T., W. Watanabe, and K. Itoh, *Laser micro-welding of silicon and borosilicate glass using nonlinear absorption effect induced by 1558-nm femtosecond fiber laser pulses - art. no. 646018.* Commercial and Biomedical Applications of Ultrafast Lasers VII, 2007. **6460**: p. 46018-46018.
67. Lacroix, F., D. Helie, and R. Vallee, *Optical Bonding Reinforced by Femtosecond Laser Welding.* Optical Manufacturing and Testing Ix, 2011. **8126**.
68. Huang, H., L.M. Yang, and J. Liu, *Direct welding of fused silica with femtosecond fiber laser.* Laser-Based Micro- and Nanopackaging and Assembly Vi, 2012. **8244**.
69. Tamaki, T., W. Watanabe, and K. Itoh, *Laser micro-welding of silicon and borosilicate glass using nonlinear absorption effect induced by 1558-nm femtosecond fiber laser pulses*, in *Commercial and Biomedical Applications of Ultrafast Lasers Vii*, J. Neev, et al., Editors. 2007.
70. Watanabe, W., et al., *Joining of transparent materials by femtosecond laser pulses*, in *Commercial and Biomedical Applications of Ultrafast Lasers Vii*, J. Neev, et al., Editors. 2007.
71. Coelho, L., et al., *Characterization of zinc oxide coated optical fiber long period gratings with improved refractive index sensing properties.* Sensors and Actuators B-Chemical, 2016. **223**: p. 45-51.
72. Yin, G.L., et al., *Simultaneous Refractive Index and Temperature Measurement With LPFG and Liquid-Filled PCF.* Ieee Photonics Technology Letters, 2015. **27**(4): p. 375-378.
73. Liu, Y., et al., *Analysis on strain sensing characteristic of long period fibre grating based on deep-grooved process.* Journal of Modern Optics, 2017. **64**(7): p. 672-680.
74. Ren, K.L., et al., *Online fabrication scheme of helical long-period fiber grating for liquid-level sensing.* Applied Optics, 2016. **55**(34): p. 9675-9679.
75. Chen, H.Y., Z.T. Gu, and K. Gao, *Humidity sensor based on cascaded chirped long-period fiber gratings coated with TiO2/SnO2 composite films.* Sensors and Actuators B-Chemical, 2014. **196**: p. 18-22.

76. Tang, J., et al., *Long Period Fiber Grating Inscribed in Hollow-Core Photonic Bandgap Fiber for Gas Pressure Sensing.* Ieee Photonics Journal, 2017. **9**(5).
77. James, S.W. and R.P. Tatam, *Optical fibre long-period grating sensors: Characteristics and application.* Measurement Science and Technology, 2003. **14**(5): p. R49-R61.
78. Kalachev, A.I., V. Pureur, and D.N. Nikogosyan, *Investigation of long-period fiber gratings induced by high-intensity femtosecond UV laser pulses.* Optics Communications, 2005. **246**(1-3): p. 107-115.
79. Fujimaki, M., et al., *Fabrication of long-period optical fiber gratings by use of ion implantation.* Optics Letters, 2000. **25**(2): p. 88-89.
80. Wang, Y.P., *Review of long period fiber gratings written by CO2 laser.* Journal of Applied Physics, 2010. **108**(8).
81. Rego, G., *Arc-Induced Long Period Fiber Gratings.* Journal of Sensors, 2016.
82. Salas-Alcantara, K.M., et al., *Modal interferometer based on a single mechanically induced long-period fiber grating and a nanoparticles-coated film section.* Optics Letters, 2017. **42**(9): p. 1780-1783.
83. Erdogan, T., et al., *DECAY OF ULTRAVIOLET-INDUCED FIBER BRAGG GRATINGS.* Journal of Applied Physics, 1994. **76**(1): p. 73-80.
84. Dong, X.R., et al., *Femtosecond laser fabrication of long period fiber gratings by a transversal-scanning inscription method and the research of its orientational bending characteristics.* Optics and Laser Technology, 2015. **71**: p. 68-72.
85. Ryu, H.S., et al., *Effect of asymmetric stress relaxation on the polarization-dependent transmission characteristics of a CO2 laser-written long-period fiber grating.* Optics Letters, 2003. **28**(3): p. 155-157.
86. Shang, R.B., et al., *Fabrication of twisted long period fiber gratings with high frequency CO2 laser pulses and its bend sensing.* Journal of Optics, 2013. **15**(7).
87. Tian, F., et al., *Long-period gratings inscribed in photonic crystal fiber by symmetric CO2 laser irradiation (vol 21, pg 13208, 2013).* Optics Express, 2015. **23**(18): p. 23570-23570.
88. Zhang, C., et al., *Long Period Fiber Grating Fabrication by Two-Step Infrared Femtosecond Fiber Laser Exposure.* Ieee Photonics Journal, 2017. **9**(4).
89. Bhatia, V., et al., *Temperature-insensitive and strain-insensitive long-period grating sensors for smart structures.* Optical Engineering, 1997. **36**(7): p. 1872-1876.
90. Wang, J.N. and C.Y. Luo, *Long-Period Fiber Grating Sensors for the Measurement of Liquid Level and Fluid-Flow Velocity.* Sensors, 2012. **12**(4): p. 4578-4593.
91. Dong, Y.Y., et al., *Novel bending sensor based on a meniscus shaped beam with LPG.* Optik, 2013. **124**(24): p. 6737-6739.
92. Sun, J., et al., *Application of an artificial neural network for simultaneous measurement of bending curvature and temperature with long period fiber gratings.* Sensors and Actuators a-Physical, 2007. **137**(2): p. 262-267.

93. Gaudron, J.O., et al., *LPG-based optical fibre sensor for acoustic wave detection.* Sensors and Actuators a-Physical, 2012. **173**(1): p. 97-101.
94. Chan, C.C., et al., *Bending measurement using embedded long-period fiber gratings.* Sensors for Harsh Environments, 2004. **5590**: p. 96-104.
95. Chan, C.C., et al., *Simultaneous measurement of curvature and temperature for LPG bending sensor.* Sensors for Harsh Environments, 2004. **5590**: p. 105-110.
96. Tanaka, S., A. Wada, and N. Takahashi, *Highly sensitive operation of LPG vibration sensor using bending-induced spectral change.* 21st International Conference on Optical Fiber Sensors, 2011. **7753**.

Publications

Cho, Y., et al., *Fabrication of a Screw-Shaped Long-Period Fiber Grating for Refractive Index Sensing.* Ieee Photonics Technology Letters, 2017. **29**(24): p. 2242-2245.

Saad, A., et al., *Numerical Approach to Modeling and Characterization of Refractive Index Changes for a Long-Period Fiber Grating Fabricated by Femtosecond Laser.* Materials, 2016. **9**(11).

Joe, H.-E., et al., *CHARACTERIZATION OF LONG PERIOD GRATING WITH A SCREW SHAPE FABRICATED BY A SINGLE-PATH SCANNING OF FEMTOSECOND LASER.* Proceedings of the Asme 13th International Manufacturing Science and Engineering Conference, 2018, Vol 4. 2018.

Bhullar, S.K., et al., *Design and fabrication of auxetic PCL nanofiber membranes for biomedical applications.* Materials Science & Engineering C-Materials for Biological Applications, 2017. **81**: p. 334-340.

Bhullar, S.K., et al., *Fabrication and Characterization of Nonwoven Auxetic Polymer Stent.* Polymer-Plastics Technology and Engineering, 2015. **54**(15): p. 1553-1559.

Ko, J., et al., *Design and fabrication of auxetic stretchable force sensor for hand rehabilitation.* Smart Materials and Structures, 2015. **24**(7).